Physics of Fluids

Vortex-induced vibrations of an elliptic cylinder of low mass ratio: Identification of new response branches

Cite as: Phys. Fluids **32**, 023605 (2020); https://doi.org/10.1063/1.5141030
Submitted: 04 December 2019 . Accepted: 04 February 2020 . Published Online: 24 February 2020

Kumar Sourav, Deepak Kumar, and Subhankar Sen

View Online Export Citation CrossMark

Scilight Highlights of the best new research in the physical sciences LEARN MORE! AIP Publishing

AIP Publishing

© 2020 Author(s).

Physics of Fluids ARTICLE scitation.org/journal/phf

Vortex-induced vibrations of an elliptic cylinder of low mass ratio: Identification of new response branches

Cite as: Phys. Fluids 32, 023605 (2020); doi: 10.1063/1.5141030
Submitted: 4 December 2019 • Accepted: 4 February 2020 •
Published Online: 24 February 2020

View Online Export Citation CrossMark

Kumar Sourav, Deepak Kumar, and Subhankar Sen[a)]

AFFILIATIONS

Department of Mechanical Engineering, Indian Institute of Technology (Indian School of Mines), Dhanbad, Dhanbad 826004, India

[a)]**Author to whom correspondence should be addressed:** ssen@iitism.ac.in. **Tel.:** +91 326 223 5188

ABSTRACT

The classical resonance branches that construct the response of a freely vibrating circular or elliptic cylinder at low Reynolds numbers, *Re*, are "initial" and "lower." The existence of additional response branches, if any at low *Re* via alteration of controlling parameters, is unavailable in the literature. In this computational work, relating to a low mass ratio ($m^* = 1$) and zero damping, i.e., $m^*\zeta = 0$ transverse-only vortex-induced vibrations of an elliptic cylinder over *Re* = 50–180, four response branches that are unreported in the literature are identified. The lock-in at such a low mass ratio is non-classical, and the new response branches are resolved close to the lock-in boundaries. These additional branches are designated as extended initial branch, extended lower branch, terminal branch, and quasi-periodic desynchronization branch. The method proposed by Kumar *et al.* ["Identification of response branches for oscillators with curved and straight contours executing VIV," Ocean Eng. **164**, 616–627 (2018b)] has been employed to identify the branches by locating the *Re* region concerning the change of slope and discontinuous jumps of oscillation frequency. It is further shown that branching at a low mass ratio depends on structural damping, oscillator shape, and degree-of-freedom.

Published under license by AIP Publishing. https://doi.org/10.1063/1.5141030

I. INTRODUCTION

A rigid or flexible obstacle mounted flexibly in a moving viscous fluid of density, ρ, interacts with the flow field in either of the two ways: one-sided interactions and mutual or two-sided interactions. In the former, the motion of the obstacle is controlled externally, and hence, the fluid medium is unable to impart any influence on the motion of the solid. Such oscillator motions where the amplitude and frequency of the oscillator enter as input variables/known quantities come under the domain of forced vibrations. Therefore, for forced vibrations, the velocity and pressure fields are the primary unknowns. In the numerical approach, these quantities are obtained by solving the Navier–Stokes equations of motion. Since the oscillator response is known beforehand, the equation of rigid body motion is not solved. In the latter, motion of the solid and fluid media is intrinsically coupled, and hence, motion of both the fluid and solid is influenced by each other. In particular, the essential no-slip boundary condition at the fluid–solid interface along with the instantaneous fluid forcing couple the governing differential equations of flow and rigid body motion. These are the instances of free or vortex-induced vibrations (VIVs). The VIV can be studied experimentally or numerically. In numerical analysis, the flow and rigid body equations can be handled simultaneously (coupled approach) or separately/sequentially (partitioned approach). The VIV is a strong function of the oscillator shape (because of its close bearing on the location of separation points) and degree-of-freedom (DOF) besides several structural and flow quantities. The influencing parameters are mostly non-dimensional and are listed as mass ratio, m^*, or relative density of the oscillator; structural damping coefficient, ζ; reduced or non-dimensional natural frequency, F_N, or reduced speed, $U^* = \frac{1}{F_N}$, of the oscillator; and Reynolds number, *Re*, of the flow. It may be noted that both oscillator shape and *Re* influence the free and forced vibrations. Since no rigid body equation is solved in forced vibrations, the quantities such as m^*, ζ, and F_N appearing in the rigid body equations [see Eqs. (6) and (7)] do not affect the forced vibrations. For a bluff oscillator with characteristic

Published under license by AIP Publishing

dimension, D (projection of the bluff body across the flow), facing a free-stream speed, U, these influencing parameters are defined as follows:

Mass ratio: the ratio of oscillator mass, m, per unit length to the mass, m_d, of displaced fluid per unit length. At a low mass ratio, the VIV is non-classical (Khalak and Williamson, 1997) as the condition of lock-in is not met, i.e., the cylinder oscillation frequency differs from (surpasses) the structural natural frequency. By low m^*, we imply, in this work, the mass ratio of unity. Such low mass ratios are encountered in marine structures (Stappenbelt *et al.*, 2007).

Structural damping coefficient: this is different from fluid damping and is given by the $\frac{c}{2\sqrt{km}}$ ratio, where c and k denote the damping and stiffness of the oscillator system, respectively.

Reduced natural frequency: the reciprocal of reduced speed or normalized free-stream speed. It is defined as $F_N = \frac{f_N D}{U}$, where f_N is the dimensional natural structural frequency of the oscillator. Thus, $U^* = \frac{U}{f_N D}$ represents the free-stream speed normalized with natural frequency and characteristic dimension.

Reynolds number: the product $\frac{UD}{\nu}$, where ν is the kinematic viscosity of the fluid. The minimum Re at which the VIV of a circular cylinder is found to exist is ≈18 (Kou *et al.*, 2017).

For oscillators of large mass ratio or $m^* \gg 1$, Bearman (1984) suggested that resonance (or lock-in or synchronization) corresponds to $F_N \approx St_0 \approx St_Y$, where St_0 is the vortex-shedding frequency of the oscillator when held stationary and St_Y is the normalized transverse oscillation frequency. St stands for the Strouhal number and signifies non-dimensional frequency. Depending on the value of U, the stationary vortex-shedding frequency approaches F_N and eventually locks onto it, rendering the structure to vibrate with St_Y, the magnitude of which is approximately equal to F_N (Blevins, 1990). This is the classical lock-in observed for moderate to large mass ratios. For a low mass ratio, such as unity, both St_Y and the vortex-shedding frequency of the oscillating cylinder, St_{C_l}, depart significantly from F_N within synchronization. Mittal and Kumar (1999; 2001) referred to this phenomenon as "soft lock-in." Under such circumstances, the lock-in becomes non-classical (Khalak and Williamson, 1999). To take into account the mismatch of St_Y and F_N within synchronization for the VIV with low m^*, Sarpkaya (1995) and Khalak and Williamson (1999) correlated the occurrence of lock-in with matching of St_Y with St_{C_l}, where St_{C_l} signifies the frequency of the periodic wake vortex mode. The quantities St_Y and St_{C_l} may, however, differ from F_N (Prasanth and Mittal, 2008). Kumar *et al.* (2016) numerically examined the relationship between St_Y and St_{C_l} in context of forced vibrations of a circular cylinder and identified three distinct regimes: lock-in, transition, and no lock-in. These regimes correspond to satisfaction of (i) $St_{C_l} = St_Y$ besides minor frequencies of lift becoming integer multiples of St_Y, (ii) $St_{C_l} = St_Y$ only, and (iii) none of (i) and (ii), respectively. This method of locating various states of vibration has been recently implemented by Jiao and Wu (2018).

This study explores the branching phenomenon of response for an elliptical oscillator of low mass ratio. Certain segments of response within and outside the regime of synchronization constitute the response curve of an oscillator and are referred to as response branches. The segment of response in the steady regime of flow (prior to the onset of vortex-shedding or due to suppression of vortex-shedding) forms the steady state (SS) regime (Navrose *et al.*, 2014) shown in Fig. 1(a) where the mean transverse force and response are both zero. The steady state regime may be composed of a pair of components [Fig. 1(b)]. The low amplitude response of an oscillator corresponding to its non-locked-in state contributes to the decoherence or desynchronization branch, DS. The DS is composed of DS I and DS II, i.e., the segments of decoherence prior to the onset of lock-in and post the lock-out, respectively (Navrose *et al.*, 2014). It is emphasized here that the desynchronization regime discussed in the literature is periodic and no description of a quasi-periodic DS regime is available. We resolve in this work, for the first time, a quasi-periodic component of DS II and designate it with the symbol DS II (QP) (see Subsection V A). The periodic part of DS II is denoted by DS II (P). The major branches that constitute the response under synchronization are initial branch, IB; upper branch, UB; and lower branch, LB (Khalak and Williamson, 1996; 1997; and 1999). The initial and lower branches are located at the lower and upper U^* (or Re) extremity of lock-in, respectively. Thus, the initial branch forms at the onset of lock-in, while the end of the lower branch

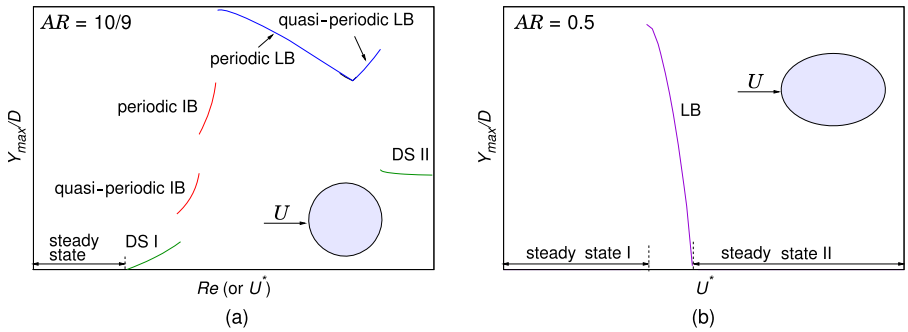

FIG. 1. Undamped free vibrations of an elliptic cylinder: (a) the relationship between response and Re (or U^*) for an elliptic cylinder of $AR = \frac{10}{9}$ (see Fig. 3 of Navrose *et al.*, 2014) and (b) modification of response when AR changes to 0.5 (see Fig. 6 of Kumar *et al.*, 2018a). For (b), the cylinder executes undamped transverse-only VIV at $Re = 100$. For $AR > 1$, the major axis is perpendicular to the flow, whereas it is parallel to the flow for $AR < 1$. Panel (a) is reproduced with permission from Navrose *et al.*, "Free vibrations of an elliptic cylinder at low Reynolds numbers," J. Fluids Struct. **51**, 55–67 (2014). Copyright 2014 Elsevier. Panel (b) is reproduced with permission from Kumar, D., Mittal, M., and Sen, S., "Modification of response and suppression of vortex-shedding in vortex-induced vibrations of an elliptic cylinder," Int. J. Heat Fluid Flow **71**, 406–419 (2018a). Copyright 2018 Elsevier.

Published under license by AIP Publishing

marks the closure of lock-in. The upper branch, located in between the IB and LB, is associated with the maximum response. While the amplitude of oscillations in the upper branch can exceed a cylinder diameter, the amplitude in the lower branch is smaller, i.e., of the order of 0.6D (Fig. 2 of Khalak and Williamson, 1999). According to Carberry *et al.* (2004) the IB, UB, and LB correspond to high, medium, and low frequency states, respectively. In Subsections I A–I C, the concepts of response branching and its development are discussed. The discussion also includes the role of parameters influencing the branching and summary of response branching. The closure of this section highlights the primary objectives of this work.

A. The origin of response branching

The most important output variable in the VIV is the maximum response in the transverse direction, Y_{max}. This is because the fluctuations in the lift force, C_l, acting across the flow surpass those in the drag force, C_d, along the flow by at least an order of magnitude. Thus, oscillations in the body are predominantly across the flow. The earliest known experimental investigation of the VIV is due to Feng (1968) at subcritical Reynolds number. For Re of the order of 10^4 and $m^*\zeta = 0.36$, he presented detailed results for transverse response of a rigid circular cylinder executing single-degree-of-freedom VIV. Here, the quantity $m^*\zeta$ (≥ 0) represents the combined mass-damping parameter. Feng (1968), however, did not explore the branching of response. Based on experimental results of the VIV of a flexible circular cable of $m^*\zeta = 0.41$ in air (implies high m^*) over Re = 3400–11 800, Brika and Laneville (1993) discussed the upper branch and lower branch of hysteresis loop (not exactly the same as the upper and lower branches of response). The concept of branching of response was more clearly introduced for the first time by Khalak and Williamson (1996) in context of transverse-only VIV of a rigid circular cylinder at high Re. They, however, did not specify the exact values of Re. For very low values of mass and damping of the oscillator system ($m^* = 2.4$, $m^*\zeta = 0.013$, thus, $\zeta = \frac{0.013}{2.4} = 0.0054$), they conducted experiments for hydroelastic vibrations in a water channel. Khalak and Williamson (1996) interpreted that the high m^* response obtained by Feng (1968) and Brika and Laneville (1993) for a circular cross section is composed of an upper branch followed by a lower branch. The response is high in the UB, and it is of moderate magnitude in the LB. Khalak and Williamson (1996) found that the decomposition of response in the upper and lower branches for high values of the combined mass-damping parameter remains valid for low values of $m^*\zeta$ (such as 0.013) as well. In a subsequent experiment at $Re \approx 6000$ using the same water channel, Khalak and Williamson (1997) revisited the transverse response of the circular cylinder for the same low m^* of 2.4 but slightly lower ζ (=0.0045). For the VIV with such low $m^*\zeta$, the U^* range of cylinder excitation quadrupled and Y_{max}/D almost doubled, as compared to the high $m^*\zeta$ results of Feng (1968). Concerning this wide regime of cylinder excitation, Khalak and Williamson (1997) identified the existence of two additional branches of response: the initial excitation regime or initial branch occurring at the onset of excitation and desynchronization (DS) or decoherence regime appearing post the closure of excitation. Overall, the response, therefore, is composed of IB, UB, LB, and DS. The transition from the IB to UB is hysteretic, while the UB to LB transition involves an intermittent switching between the UB and LB. They further subdivided the IB into two sub-branches: the quasi-periodic initial branch at lower U^* and the periodic initial branch at relatively higher U^*. The earlier decomposition of Feng (1968) and Brika and Laneville (1993) response into the UB and LB by Khalak and Williamson (1996) was later replaced by decomposition into the IB and LB by Khalak and Williamson (1999) where they classified the response of a circular cylinder into two families based on the magnitude of $m^*\zeta$. In the first family of response corresponding to low $m^*\zeta$, the response consists of IB, UB, and LB, while for the second family at high $m^*\zeta$, it comprises IB and LB. It may be noted that the range of Re considered by Khalak and Williamson (1999) is 3500–10 000. They conjectured that the value of $m^*\zeta$ mainly governs the presence or absence of the upper branch. Through experimental observations, Klamo *et al.* (2006) demonstrated that a combination of high Re and low $m^*\zeta$ is linked to the formation of UB. By conducting three-dimensional numerical experiments for $m^* = 50.8$ and $m^*\zeta = 0.122$, Blackburn *et al.* (2000) resolved the upper branch of response for a much lower Reynolds number range of the order of 500. The response curves presented by Anagnostopoulos and Bearman (1992) in Figs. 2 and 8 (for increasing Re) and Fig. 9 (for decreasing Re) of their paper suggests that the response for Re = 90–150 comprises the IB, LB, and DS regimes; the UB does not appear. Anagnostopoulos and Bearman (1992) conducted VIV experiments in a water channel for a circular rod of $m^* = 0.004\,27$. Zhu *et al.* (2019) numerically investigated the damped ($\zeta = 0.01$) VIV of a circular cylinder of $m^* = 1$ at $Re = 100$ and resolved the IB, LB, and DS. Numerical investigations at low Re by Singh and Mittal (2005) and Prasanth and Mittal (2008) for $m^* = 10$ and zero damping ascertain that the response is composed of IB, LB, and DS regimes. Using two-dimensional computations for the VIV of a circular cylinder of $m^* = 10$ at $Re = 200$, Leontini *et al.* (2006) resolved two response branches that are similar in nature to the upper and lower branches captured in three-dimensional flow. It may be noted that branching in the synchronization regime was not discernible from response but from other VIV parameters.

As a counterpart of the upper branch corresponding to transverse-only VIV of a circular cylinder, Williamson and Jauvtis (2004) identified, for $m^* = 2.6$, a new high amplitude response branch when the cylinder executes two-degrees-of-freedom (2-DOF) VIV, i.e., simultaneous in-line and cross-stream VIV. This branch, where the value of the maximum transverse response equals three times the cylinder diameter, was named as the "super-upper branch," SUB by them. The water channel experiments were conducted for Re = 1000–15 000, and the mass-damping parameter was varied from 0.001 to 0.01.

B. Factors influencing the branching

As apparent from the above discussion, the branching of response depends on the degree-of-freedom as well as the values of $m^*\zeta$ and Re. Another important influencing parameter is the shape of the oscillator. For aeroelastic vibrations of a square cylinder of high mass-damping parameter ($m^*\zeta = 905 \times 0.000\,828 = 0.7493$) over Re = 2000–8000, Amandolese and Hemon (2010) interpreted their response curve to be composed of IB and LB. A close inspection of their response curve however, reveals that it is composed of IB, LB, DS, and galloping branch, GB. GB is characteristic to non-axisymmetric cross sections and hence is absent in the response of an isolated circular cylinder. For 2-DOF undamped vortex-induced

Published under license by AIP Publishing

motion of a square cylinder of $m^* = 10$ (here, $m^*\zeta = 0$) and $60 \le Re \le 250$, Sen and Mittal (2011) found that the response is composed of IB, LB, and DS regimes and GB. For high Re and low $m^*\zeta$, Nemes *et al.* (2012) (using $m^*\zeta = 0.00649$) and Zhao *et al.* (2014) (using $m^*\zeta = 0.00681$) experimentally explored the branching of a freely vibrating square cylinder for various angles of incidence bounded by 0° and 45°. For zero incidence, Nemes *et al.* (2012) found that the motion is composed of VIV and galloping, but they did not explore the branching in the VIV regime. For 45° incidence, the branching is similar to that of a circular cylinder, i.e., IB, UB, LB, and DS constitute the response. A new branch with maximum response surpassing even that of the UB was noted when the angle of incidence ranged between 10° and 22.5°. They coined the term "higher branch," HB, to denote this branch. Zhao *et al.* (2014) identified the IB, UB, and DS regimes for the zero angle of attack. They provide finer details of the UB, but identification of the LB is not clear. For 20° incidence, they identified the HB that was first noted by Nemes *et al.* (2012). The response comprised IB, UB, HB, and DS regimes. Interestingly, the LB appears to be absent. In context of undamped VIV of elliptic cylinders of various aspect ratios, AR (ratio of lengths of the major and minor axes of an elliptic cylinder), in the laminar vortex-shedding regime (Re = 60–140), Navrose *et al.* (2014) provided a detailed account of response branching. Depending on the aspect ratio of a cylinder, they found that a regime of steady state exists in the vicinity of the lowest Re considered. A regime of desynchronization, designated as DS I by them, follows thereafter. The standard DS regime, thus, reduces to the second regime of desynchronization or DS II. They further sub-divided the LB in its periodic and quasi-periodic components. Figure 1(a) (after Navrose *et al.*, 2014) illustrates all the possible branching of response for low Re undamped VIV of an elliptic cylinder of $AR = \frac{10}{9}$. Further simplification of this branching was recently reported by Kumar *et al.* (2018a) in context of undamped VIV of an elliptic cylinder of $AR = 0.5$ at $Re = 100$. They observed that the response for such a thin cylinder is composed of the LB and two regimes of the steady state, i.e., steady state I and steady state II [Fig. 1(b)]. The IB, DS I, and DS II regimes do not exist. It may be noted that the major axis of the elliptic cylinder is normal to the incoming flow for $AR > 1$, while for $AR < 1$, it is parallel to the flow.

C. Summary of response branching

For oscillators with smooth contours and straight edges (e.g., a circular cylinder and a square cylinder at incidence), the first and second columns of Fig. 2, respectively, illustrate the response branching subject to various input conditions. Figures 2(a) and 2(b) depict the response branching due to Khalak and Williamson (1999) for transverse-only VIV of a circular cylinder of high and low values of the combined mass-damping parameter, $m^*\zeta$, respectively. Irrespective of the values of m^* and ζ (Bahmani and Akbari, 2010), Fig. 2(a) is also valid for SDOF or 2-DOF VIV of a circular cylinder at low Re. Inclusion of the in-line degree-of-freedom induces further alterations of response branching as illustrated in Fig. 2(c) (Jauvtis and Williamson, 2004). In Fig. 2(c), SS and AS stand for streamwise symmetric and streamwise anti-symmetric, respectively. For a square cylinder at zero incidence, Fig. 2(d) depicts the branching for low as well as high mass ratios. For $Re \ge 150$ and $U^* \ge 10$, the galloping branch is absent if $m^* < 4$ and all the branches become present when $m^* \ge 4$, approximately (Li *et al.*, 2019). As already stated, Zhao *et al.* (2014) resolved the initial, upper, and higher branches and the desynchronization regime for flow-induced transverse-only vibrations of a square cylinder at 20° incidence and high Re [Fig. 2(e)]. For transverse-only VIV of a square cylinder at 45° incidence, i.e., a diamond cylinder, the response [Fig. 2(f)] at low Re, such as 100, consists of the initial and lower branches and desynchronization regimes (Sourav *et al.*, 2020). Figure 2, therefore, illustrates the effects of geometry (first and second columns of this figure), combined mass-damping parameter [Figs. 2(a) and 2(b)],

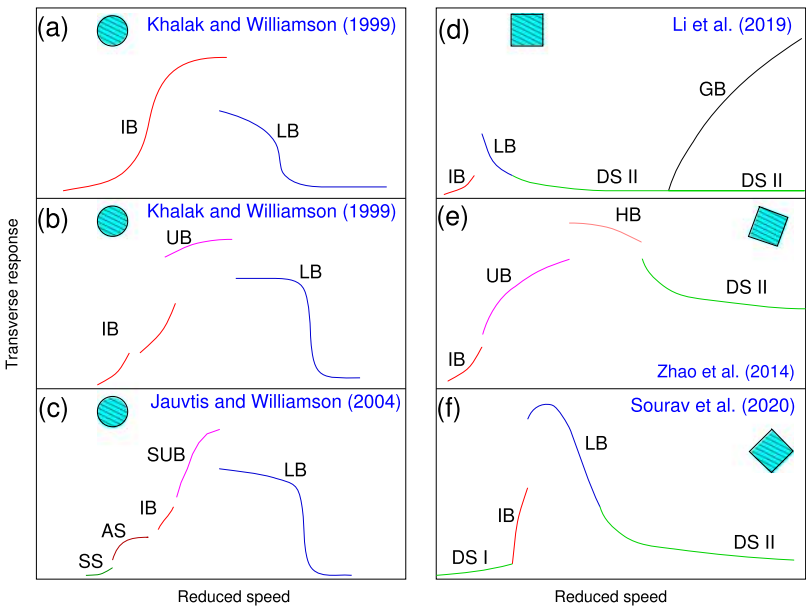

FIG. 2. Illustration of classical response branches for oscillators with smooth contours (first column) and straight edges (second column) executing free vibrations: (a) Y-only motion of a circular cylinder of high $m^*\zeta$ (Khalak and Williamson, 1999), (b) Y-only motion of a circular cylinder of low $m^*\zeta$ (Khalak and Williamson, 1999), (c) X–Y motion of a circular cylinder of low $m^*\zeta$ (Jauvtis and Williamson, 2004), (d) Y-only motion of a square cylinder at zero incidence (Li *et al.*, 2019) showing both VIV and galloping, (e) Y-only motion of a square cylinder of $m^* = 2.4$ at 20° incidence (Zhao *et al.*, 2014), and (f) undamped Y-only motion of a square cylinder of $m^* = 10$ at 45° incidence (Sourav *et al.*, 2020).

Published under license by AIP Publishing

TABLE I. Summary of response branching for oscillators of various cross sections.

Study	Cross section	Input parameters	Response branches
Feng (1968)	Circle	$Re = O(10^4)$, $m^*\zeta = 0.36$, Y-only	...
Anagnostopoulos and Bearman (1992)	Circle	$Re = 90$–150, $m^* = 0.004\,27$, Y-only	IB, LB, and DS
Brika and Laneville (1993)	Circle	$Re = 3\,400$–$11\,800$, $m^*\zeta = 0.41$, Y-only	UB and LB
Khalak and Williamson (1996)	Circle	$m^* = 2.4$, $m^*\zeta = 0.013$, Y-only	UB and LB
Khalak and Williamson (1997)	Circle	$Re \approx 6\,000$, $m^* = 2.4$, $\zeta = 0.004\,5$, Y-only	IB, UB, LB, and DS
Khalak and Williamson (1999)	Circle	$Re = 3\,500$–$10\,000$, Y-only Low $m^*\zeta$ [$=O(0.01)$], High $m^*\zeta$ [$=O(0.1)$]	IB, UB, and LB IB and LB
Blackburn *et al.* (2000)	Circle	$Re \approx 500$, $m^* = 50.8$, $m^*\zeta = 0.122$, Y-only	IB, UB, and LB
Jauvtis and Williamson (2004)	Circle	$Re = 1\,000$–$15\,000$, $m^*\zeta = 0.001$–0.01, X–Y	IB, SUB, LB, and DS
Singh and Mittal (2005)	Circle	$Re = 50$–500, $m^* = 10$, $\zeta = 0$, X–Y	IB, LB, and DS
Klamo *et al.* (2006)	Circle	$Re = 525$–$2\,600$, $m^* = 7.1$–156.7, $\zeta = 0.016$–0.977, Y-only	IB, UB, LB, and DS
Prasanth and Mittal (2008)	Circle	$Re = 60$–200, $m^* = 10$, $\zeta = 0$, X–Y	IB, LB, and DS
Amandolese and Hemon (2010)	Square (0°)	$Re = 2\,000$–$8\,000$, $m^*\zeta = 0.749\,3$, Y-only	IB and LB
Sen and Mittal (2011)	Square (0°)	$Re = 60$–250, $m^* = 10$, $\zeta = 0$, X–Y	IB, LB, DS, and GB
Nemes *et al.* (2012)	Circle Square (0°) Square (20°) Square (45°)	$Re = 2\,500$–$12\,500$, $Re = 2\,500$–$12\,500$, $U^* = 2$–18, $m^* = 2.2$, $\zeta = 0.006\,49$, Y-only	IB, UB, and LB ... IB, UB, HB, and DS IB, UB, LB, and DS
Zhao *et al.* (2014)	Square (0°) Square (20°) Square (45°)	$Re = 2\,000$–$13\,000$, $U^* = 2.75$–17, $m^* = 2.64$, $\zeta = 0.002\,58$, Y-only	... IB, UB, HB, and DS IB, UB, and DS
Navrose *et al.* (2014)	Ellipse	$Re = 60$–140, $AR = 0.7$–1.43, $m^* = 10$, $\zeta = 0$, X–Y	Steady state, DS I, IB (QP), IB (P), LB (P), LB (QP), and DS II
Kumar *et al.* (2018a)	Ellipse	$Re = 100$, $m^* = 10$, $\zeta = 0$, Y-only	Steady state I, LB, steady state II
Kumar *et al.* (2018b)	Circle Square (0°) Ellipse D-section	$Re = 60$–150, $m^* = 1$, 10, $AR = 0.9$, 1, 1.11, $\zeta = 0$, X–Y	DS I, IB, LB, DS II DS I, LB, DS II DS I, IB, LB, and DS II DS I, IB, LB, and DS II
Sourav and Sen (2019)	Square (0°)	$Re = 60$–250, $m^* = 3.3$–4 $\zeta = 0$, X–Y	DS I, IB, LB, DS II, GB
Sourav *et al.* (2020)	Square (45°)	$Re = 100$, $U^* = 1$–12, $m^* = 10$, $\zeta = 0$, Y-only	DS I, IB, LB, DS II
Present	Ellipse	$Re = 50$–180, $AR = 1.11$, $m^* = 1$ $\zeta = 0$, Y-only $\zeta = 0.044$, Y-only $\zeta = 0$, X–Y	DS I, IB, LB, ELB, TB, DS II (QP), DS II (P) DS I, IB, LB, ELB, DS II DS I, IB, EIB, LB, DS II

Published under license by AIP Publishing

degree-of-freedom [Fig. 2(c)], mass ratio, Re, and U^* [Fig. 2(d)], and angle of incidence [Figs. 2(e) and 2(f)]. The branching of a circular cylinder further alters if the aspect ratio of the cylinder differs from unity, i.e., the cylinder shape becomes elliptic (Navrose *et al.*, 2014 for $60 \le Re \le 140$). An extensive summary of response branching is provided in Table I. This table also includes the new branches, such as Extended Initial Branch (EIB), Extended Lower Branch (ELB), Terminal Branch (TB), and Quasi-periodic second regime of desynchronization [DS II (QP)] resolved in this work. In Table I, (QP) and (P) signify the quasi-periodic and periodic segments of a branch, respectively.

D. Objectives of the current work

The variation of angle of incidence or aspect ratio amounts to change in the oscillator shape. The above discussion, therefore, establishes that besides DOF, $m^*\zeta$, and Re, the oscillator shape is also a key influencing parameter affecting the branching. The construction of response branching is a strong function of the value of $m^*\zeta$ (Govardhan and Williamson, 2000). For the VIV of a circular cylinder over Re = 80–160, Table 2 of Bahmani and Akbari (2010) demonstrates that different combinations of m^* and ζ for identical values of $m^*\zeta$ affect the maximum response and range of lock-in. A quest, therefore, arises naturally: Do the components of $m^*\zeta$, i.e., m^* and ζ, individually influence the response branching? For Re = 50–250, Sen and Mittal, 2015; noted that the response of an undamped square cylinder comprises IB, LB, and DS regimes and GB for $m^* > 5$ and the GB does not appear for $m^* = 1$. This study, though restricted to Re = 250, suggests that m^* individually is indeed a parameter to alter the branching. Klamo *et al.* (2006) experimentally investigated the role of structural damping on the response and frequency characteristics. They varied ζ from 0.0005 to 0.0410 and a set of three mass ratios, i.e., m^* = 7.1, 78.3, and 156.7, was considered. For Re = 525–2600, decreasing ζ caused a decay in the amplitude of the UB and also shortened its extent. The effect of damping on response was investigated by Sun *et al.* (2016) for the VIV of a rough circular cylinder at Re = 30 000–120 000. The components of response were IB, UB, LB, and DS regimes and GB. They observed that increasing damping reduces the extent of the VIV regime, advances the occurrence of GB, and overall decreases the response in all branches. Thus, no fundamental modification of branching due to damping is seen from the studies of Klamo *et al.* (2006) and Sun *et al.* (2016). It is, therefore, interesting to see if the damping effects alter the branching at low Re and low m^*.

As discussed, the details of response branching concerning 2-DOF VIV for an elliptic cylinder of $AR = \frac{10}{9}$ and $m^* = 10$ were presented by Navrose *et al.* (2014). The response is composed of SS, DS I, IB (quasi-periodic and periodic), LB (periodic and quasi-periodic), and DS II. The response of this cylinder is known to be devoid of GB. The $AR = \frac{10}{9}$ cylinder is considered in this study since all the basic branches exist in its response. An Re range of 50–180, in which the flow is known to belong to the laminar vortex-shedding regime, is used. The initial question that we address is as follows: Does the branching of response for undamped 2-DOF VIV alter if m^* is lowered down to 1? The answer to this is found to be affirmative (see Subsections V A and V B). Identification of a new branch provides us the basis to explore the VIV with this mass ratio of unity subject to varying conditions. The pioneering studies by Khalak and Williamson (1996; 1997; and 1999) defining response branches relate to damped transverse VIV of low m^* (thus, $m^*\zeta \neq 0$) cylinders at high Re. The identification of a super-upper branch by Williamson and Jauvtis (2004) establishes degree-of-freedom as a parameter controlling branching. Through the findings by Khalak and Williamson (1996; 1997; and 1999) and Williamson and Jauvtis (2004), it appears to one that ζ and degrees-of-freedom may be factors to alter the response branching. We, thus, explore the independent effects of degree-of-freedom, ζ, and, in addition, cylinder shape on the response.

In this work, we have followed the method proposed by Kumar *et al.* (2018b) for identifying the response branches and associated transitions. They demonstrated that, irrespective of oscillator cross section, changes in the slope of oscillation frequency, St_Y, in the St_Y vs Re (or U^*) profile mark a transition from one response branch to another. Such transitions are difficult to identify from the

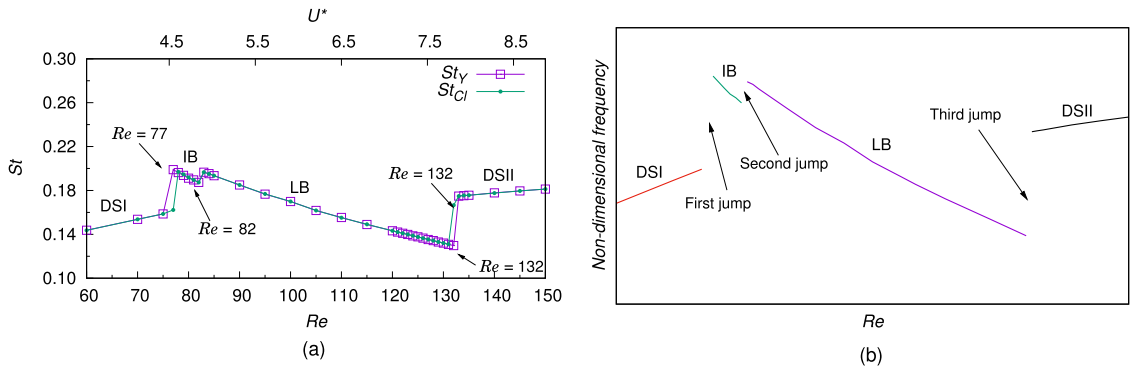

FIG. 3. Undamped 2-DOF free vibrations of an elliptic cylinder of $AR = \frac{10}{9}$ (major axis normal to the flow) and $m^* = 10$ over Re = 60–150: (a) the variation of oscillation and shedding frequencies with Re (or U^*) [see Fig. 9(c) of Kumar *et al.*, 2018b] and (b) identification of corresponding response branches and jumps in non-dimensional frequency represented by St [see Fig. 3(b) of Kumar *et al.*, 2018b]. The response for this case is shown later in Fig. 12(f). Panels (a) and (b) are reproduced with permission from Kumar, D., Singh, A. K., and Sen, S., "Identification of response branches for oscillators with curved and straight contours executing VIV," Ocean Eng. **164**, 616–627 (2018b). Copyright 2018 Elsevier.

Published under license by AIP Publishing

response of oscillators with low mass ratios or oscillators containing straight edged contours. For $AR = \frac{10}{9}$ and $m^* = 10$, Figs. 9(c) and 3(b) of Kumar *et al.* (2018b), respectively, illustrated the dependence of oscillation and vortex-shedding frequencies on Re as well as branching of response. These figures are reproduced in this paper as Figs. 3(a) and 3(b), respectively. In Fig. 3(a), St is the Strouhal number signifying the normalized frequency. The vortex-shedding frequency is denoted by St_{C_l}. As obvious from Figs. 3(a) and 3(b), the response of the $AR = \frac{10}{9}$ elliptic cylinder with $m^* = 10$ comprises DS I, IB, LB, and DS II. The initial segment of response stretching linearly up to $Re = 77$ is the DS I branch. The first change of slope of St_Y at $Re = 78$ and associated with a jump discontinuity indicates the transition to IB as well as commencement of synchronization/lock-in. The transition of IB to LB at $Re = 83$ is associated with the second slope change of St_Y as well as the second discontinuous jump. Finally, the onset of regime of desynchronization/decoherence or DS II relates to the third change of slope of the oscillation frequency curve at $Re = 133$.

The remaining of this article is organized as follows: the governing equations for incompressible fluid flow and motion of rigid body are discussed in Sec. II. Section III contains brief description of the space-time finite-element formulation. The problem statement is detailed in Sec. IV. The main results are presented in Sec. V. The appearance of four new low amplitude response branches close to the lock-in boundaries, one of them near the onset and remaining three close to the lock-out are noted. Finally, few concluding statements are given in Sec. VI.

II. THE GOVERNING EQUATIONS

A. The incompressible flow equations

Let the time-varying spatial domain and the temporal domain are denoted by $\Omega_t \subset IR^2$ and $(0, T)$, respectively. Let $\Gamma_t = (\Gamma_t)_g \cup (\Gamma_t)_h$ denote the boundary of Ω_t and is piecewise smooth. $(\Gamma_t)_g$ and $(\Gamma_t)_h$ denote the parts of boundary with the prescribed essential (Dirichlet) and natural (flux or Neumann) boundary conditions, respectively. The spatial and temporal coordinates are denoted by $\mathbf{x} = (x, y)$ and t, respectively. In strong form, the Navier–Stokes equations of motion governing incompressible flow are

$$\rho\left(\frac{\partial \mathbf{u}}{\partial t} + \mathbf{u}\cdot\nabla\mathbf{u}\right) - \nabla\cdot\boldsymbol{\sigma} = 0 \quad \text{on } \Omega_t \times (0, T), \tag{1}$$

$$\nabla\cdot\mathbf{u} = 0 \quad \text{on } \Omega_t \times (0, T). \tag{2}$$

In the above stress–divergence presentation of the Navier–Stokes equations of motion, $\mathbf{u} = (u, v)$ and $\boldsymbol{\sigma}$ are the fluid velocity vector at a point and stress tensor, respectively. The constitutive relation for the stress tensor at a point in terms of its isotropic and deviatoric components reads as

$$\boldsymbol{\sigma} = -p\mathbf{I} + \mathbf{T}, \quad \mathbf{T} = 2\,\mu\boldsymbol{\varepsilon}(\mathbf{u}), \quad \boldsymbol{\varepsilon}(\mathbf{u}) = \frac{1}{2}((\nabla\mathbf{u}) + (\nabla\mathbf{u})^T), \tag{3}$$

where p, $\mathbf{I}$, $\mathbf{T}$, μ, and $\boldsymbol{\varepsilon}$ are the pressure, identity tensor, viscous or deviatoric stress tensor, dynamic viscosity of the fluid, and strain rate tensor, respectively. Both the essential and natural boundary conditions are considered. The initial condition on the velocity is

$$\mathbf{u}(\mathbf{x}, 0) = \mathbf{u}_0 \quad \text{on } \Omega_0, \tag{4}$$

where $\mathbf{u}_0$ is divergence-free, i.e., $\mathbf{u}_0$ satisfies the condition of zero-dilatation enforced by the incompressibility constraint or conservation of mass [Eq. (2)].

B. Equations of motion for an elastically mounted rigid elliptic cylinder

Simultaneous in-line and cross-stream (or two-degrees-of-freedom) translations of an oscillator are governed by Newton's second law of motion expressed along the streamwise and cross-stream directions, respectively, as

$$m\left(\frac{d^2X}{dt^2}, \frac{d^2Y}{dt^2}\right) + c\left(\frac{dX}{dt}, \frac{dY}{dt}\right) + k(X, Y) = F_x(t), F_y(t) \quad \text{for}(0, T). \tag{5}$$

Equation (5) represents a pair of uncoupled dimensional ordinary differential equations of motion. The terms in the left-hand side represent the inertia force, viscous damping, and restoring force, respectively. The instantaneous fluid forcing terms $F_x(t)$ and $F_y(t)$ on the right-hand side act at the no-slip fluid–solid interface and couple the flow and rigid body equations. The quantities $X(t)$ and $Y(t)$ are the streamwise and transverse degrees-of-freedom or displacements of the oscillator, respectively, measured from the origin of the fixed coordinate system (discussed in Sec. IV). The rigid elliptic section oscillator is flexibly mounted and fully immersed in a moving viscous fluid [Fig. 4(a)]. The major axis of the cylinder is normal to the incoming flow. Normalization of the spatial scales is performed by the characteristic dimension, D. Here, D is the

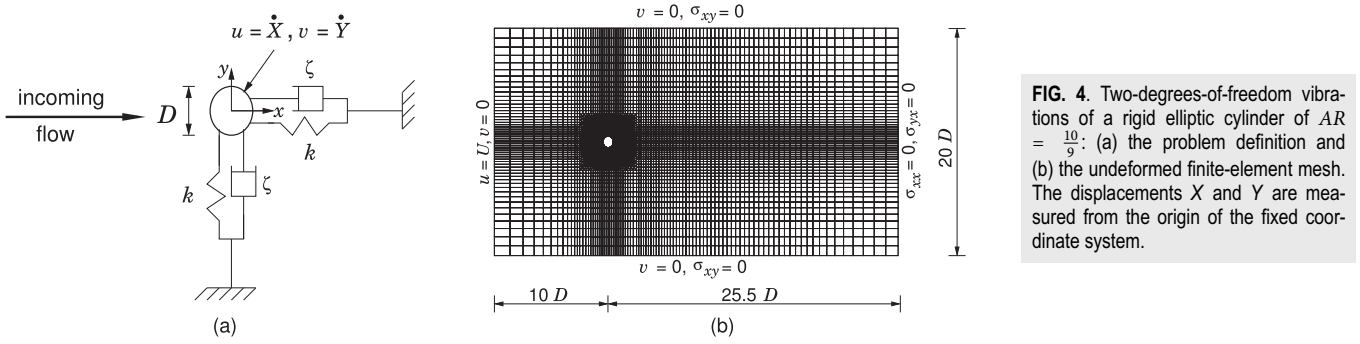

FIG. 4. Two-degrees-of-freedom vibrations of a rigid elliptic cylinder of $AR = \frac{10}{9}$: (a) the problem definition and (b) the undeformed finite-element mesh. The displacements X and Y are measured from the origin of the fixed coordinate system.

Published under license by AIP Publishing

length of major axis of the cylinder. The temporal scale is normalized by U and D. The instantaneous drag and lift coefficients are defined as $C_d(t) = \frac{F_x(t)}{0.5\rho U^2 D}$ and $C_l(t) = \frac{F_y(t)}{0.5\rho U^2 D}$, respectively. After non-dimensionalization (see Sourav and Sen, 2017), the equations of rigid body translation along and across the flow, obtained from Eq. (5), reduce to

$$\frac{d^2X^*}{dt^{*2}} + 4\pi F_N \zeta \frac{dX^*}{dt^*} + (2\pi F_N)^2 X^* = \frac{2C_d}{\pi m^*} AR \quad \text{for} \quad \left(0, \frac{TU}{D}\right), \tag{6}$$

$$\frac{d^2Y^*}{dt^{*2}} + 4\pi F_N \zeta \frac{dY^*}{dt^*} + (2\pi F_N)^2 Y^* = \frac{2C_l}{\pi m^*} AR \quad \text{for} \quad \left(0, \frac{TU}{D}\right), \tag{7}$$

where the normalized response and time are defined as $X^* = \frac{X}{D}$, $Y^* = \frac{Y}{D}$ and $t^* = \frac{tU}{D}$, respectively. From the definition of reduced speed, one gets $U^* = \frac{U}{f_N D} = \frac{UD}{\nu}\frac{1}{f_N D}\frac{\nu}{D} = \frac{\nu}{f_N D^2} Re$. For a given setup of the oscillator system, ν, f_N, and D are fixed. Therefore, U^* is linearly and F_N inversely proportional to the Reynolds number. Hence, U^* (or F_N) can be coupled with Re. To evaluate the constant of proportionality, $Re = 100$ is chosen as a reference Reynolds number since the study involves an Re range of 50–180. The stationary vortex-shedding frequency (=0.1691) of the $AR = \frac{10}{9}$ cylinder at $Re = 100$ is matched with the reduced natural frequency of the vibrating cylinder at $Re = 100$. Accordingly, the value of F_N at $Re = 100$ equals 0.1691. From this, $F_N = 0.1691 = 0.1691\frac{100}{100} = 0.1691\frac{100}{Re}$ (since F_N is inversely proportional to Re) $\Rightarrow F_N = \frac{16.91}{Re}$ or $Re = 16.91U^*$. Such interdependence of key influencing (input) parameters Re and U^* is obvious from the experimentally obtained response and frequency plots by Anagnostopoulos and Bearman (1992). This kind of relationship has been employed previously by Blackburn *et al.* (2000), Willden and Graham (2006), Prasanth and Mittal (2008), and Bahmani and Akbari (2010), among others, to compute the VIV of a circular cylinder.

The springs [see Fig. 4(a)] are assumed to be linear and identical along the directions of cylinder motion implying stiffness, $k_x = k_y = k$ (Jauvtis and Williamson, 2003). The spring stiffness that appears in the dimensional rigid body equation of motion [Eq. (5)] contributes to the dimensionless coefficient term $(2\pi F_N)^2$ appearing in the last term of the right-hand side of normalized rigid body [Eqs. (6) and (7)]. For the present computations, Re is the input variable rendering the values of $F_N = \frac{16.91}{Re}$ or $U^* = \frac{1}{F_N}$ being specified *a priori*. The relationship between the reduced natural frequency and spring stiffness is obtained as $F_N = f_N\frac{D}{U} = \frac{1}{2\pi}\sqrt{\frac{k}{m}}\frac{D}{U}$. Thus, the specification of Re, U^*, or F_N indirectly specifies the value of k. In particular, $k = m(2\pi F_N \frac{U}{D})^2$, where $F_N = \frac{16.91}{Re}$.

III. THE FINITE-ELEMENT FORMULATION

A stabilized space-time finite-element formulation incorporating the same order (here, bilinear) of interpolation for the flow variables, i.e., velocity and pressure, is used in this study. The equations for rigid body motion are also analyzed using the space-time formulation. The interpolation functions for $\mathbf{u}$ and p are bilinear in space and linear in time. Globally, these interpolation functions are continuous in space but discontinuous in time. The details of the space-time method can be found in Tezduyar *et al.* (1992a; 1992b).

IV. THE PROBLEM STATEMENT

Figure 4(a) depicts the problem setup for a symmetric rigid elliptic cylinder of $AR = \frac{10}{9}$ executing free undamped translations simultaneously along and across the flow. The cylinder is mounted flexibly in the fluid domain. An inertial or fixed frame of reference is used for analysis of the cylinder motion. At impending motion, the origin of this reference frame and the center of the cylinder coincide at (0, 0). Both undamped ($\zeta = 0$ or $m^*\zeta = 0$) and damped ($\zeta = 0.044$ or $m^*\zeta = 0.044$) free vibrations are investigated. The springs are linear, and the value of spring stiffness is identical along and across the flow. A rectangular computational domain of length $35.5D$ and width $20D$ [exterior boundary of the mesh shown in Fig. 4(b)] is truncated from the fluid domain. With this setup, the blockage or ratio of the oscillator width to the width of the truncated domain equals 0.05. Relative to the origin of the fixed (x, y) coordinate system, the upstream and downstream boundaries are located at distances of $10D$ and $25.5D$, respectively. The boundary conditions employed are free-stream inlet, slip side boundaries, stress-free exit, and no-slip at the fluid–cylinder interface. The no-slip condition on velocity at the cylinder surface is dynamic or time-dependent. Besides fluid loading, the no-slip condition also imposes a coupling between the fluid and solid media. A five-blocked (one interior or central block and four surrounding blocks) and structured non-uniform mesh composed of bilinear quadrilateral elements is used for domain discretization. The mesh consists of 7437 nodes and 7236 bilinear quadrilateral elements. To take into account the motion of the cylinder, the mesh is reconstructed at each time step. The interior block accommodates the oscillator and travels along with it as a unit. During remeshing, the location of the outer rectangular boundary and coordinate system remains fixed relative to time. However, the location of each node, except for the four corners of the domain, changes. The mesh shown in Fig. 4(b) is undeformed.

V. RESULTS

To the authors' best knowledge, there exists only a couple of studies in the literature on low Re VIV of an elliptic cylinder of low mass ratio ($m^* \approx 1$). One of these studies, i.e., Sourav and Sen (2017) for damped as well as undamped VIV of an $m^* = 1$ elliptic cylinder of $AR = \frac{10}{9}$, focused on the response characteristics. This study, however, did not explore its branching using the frequency and hence could not capture minute details of the response, particularly toward the closure of lock-in. The other study by Leontini *et al.* (2018) for $AR = 1.5$ and $m^* = 1$ delves with the evolution of wake modes with varying angles of incidence at $Re = 200$.

For certain combinations of degree-of-freedom, mass ratio, damping, and AR, two-dimensional computations are carried out over $Re = 50$–180. The focus is primarily on the $m^* = 1$ cylinder. At each time step, the asymmetric flow matrix is solved using the Generalized Minimal RESidual (GMRES) iterative equation solver due to Saad and Schultz (1986). The solution of the ordinary differential equations for rigid body motion follows a numerical integration technique (Mittal and Tezduyar, 1994). The mesh convergence and validation are discussed in detail in Sourav and Sen (2017).

Published under license by AIP Publishing

A. Undamped *Y*-only VIV of $AR = \frac{10}{9}$ elliptic cylinder with $m^* = 1$

In this subsection, we investigate, for the first time, the construction of response branching for an $AR = \frac{10}{9}$ elliptic cylinder of $m^* = 1$ executing undamped transverse-only VIV.

1. Identification of new branches ELB, TB, and DS II (QP)

The oscillation and vortex-shedding frequencies are plotted together in Fig. 5(a), while Fig. 5(b) depicts the discontinuous jumps as well as slope changes in the oscillation frequency and, finally, the identified six response branches. A total of five slope changes at Re = 53, 65, 149, 155, and 155.2, respectively, and three discontinuous jumps at Re = 53, 155, and 155.2, respectively, relate to a total of six response branches. From this lot, two response branches and a quasi-periodic segment of DS II are identified for the first time. As one moves toward the upper end of desynchronization, the order of appearance of the branches is DS I, IB, LB, ELB, TB, and DS II, where the DS II is further decomposed as DS II (QP) and DS II (P) segments. The newly identified branches are the extended lower branch (ELB), terminal branch (TB), and quasi-periodic second desynchronization branch [DS II (QP)]. Figures 5(a) and 5(b) reveal stark disparity with the one for undamped 2-DOF VIV of the same elliptic cylinder with a higher mass ratio of 10 (shown in Fig. 3). The disparity in the form of fundamental modifications of the standard frequency diagram is most prominent toward the closure of synchronization [shaded region in Fig. 5(a)]. In this "V"-shaped region, the frequency curve undergoes two additional slope changes and a pair of discontinuous jumps underscoring the existence of two intermediate branches, i.e., ELB and TB between the lower branch and DS II. No reference of such intermediate branches with low amplitude of oscillations (because of the proximity of upper boundary of lock-in) is available in the literature in context of VIV at low Re.

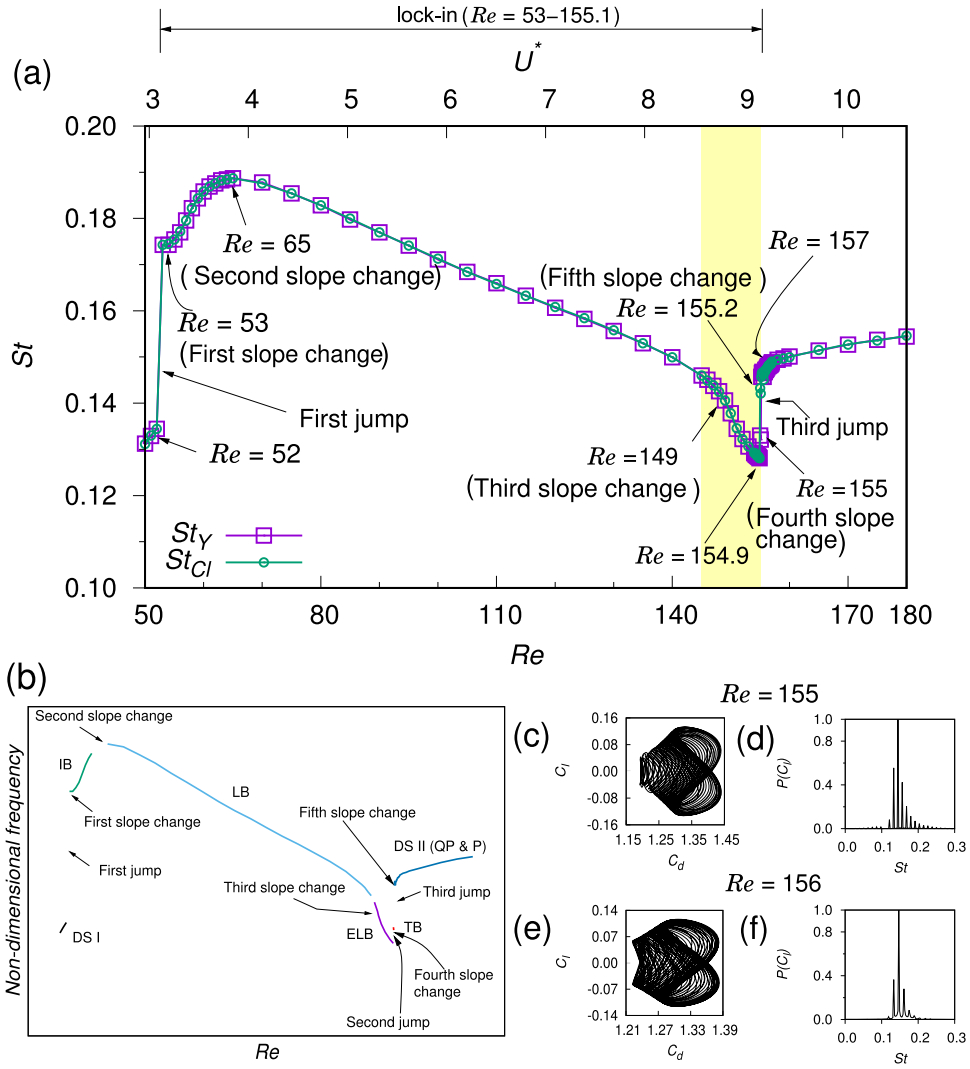

FIG. 5. Undamped *Y*-only free vibrations of an $AR = \frac{10}{9}$ and $m^* = 1$ elliptic cylinder (major axis normal to the flow): (a) the variation of oscillation and shedding frequencies with Re (or U^*), (b) further detailed presentation of (a) showing all the branches, (c) C_d–C_l phase plot at Re = 155, (d) power spectrum of C_l at Re = 155, (e) C_d–C_l phase plot at Re = 156, and (f) power spectrum of C_l at Re = 156. Re = 155 and 156 belong to TB and DS II (QP), respectively.

Published under license by AIP Publishing

The DS I continues up to Re = 52 and the first change of slope of the frequency curve occurs at Re = 53. At this Reynolds number, the DS I transits to IB. The associated jump discontinuity suggests that the onset of IB also marks the onset of synchronization. The next transition occurs at Re = 65, where St_Y (or St_{C_l}) attains its peak value of 0.1887. The third change of slope of St_Y occurs at Re = 149, and St_Y continues to undergo smooth decay post the third change of slope. This transition marks the identification of a new response branch next to the LB (and forms the V region) that we denote as "extended lower branch" (ELB). The extreme point of the ELB at Re = 154.9 corresponds to the attainment of the minimum value of St_Y or St_{C_l} (=0.1281) for the entire range of Re considered. For oscillators with a higher mass ratio, such as 10, the least value of St signifies the termination of lock-in (Kumar *et al.*, 2018b). For m^* = 1, the minimum frequency, however, is not an indicator of the closure of lock-in but an indicator of the upper limit of the ELB. The second jump (of small magnitude) in St_Y at Re = 155 and associated fourth change of slope marks the existence of a new branch that is separated from the lower branch or its extension. This is the final resonance branch and is accordingly referred to as the terminal branch (TB). The TB stretches over an extremely narrow Re interval of 155–155.1. The magnitude of St_Y slightly rises in the TB. A discontinuous (third) jump of frequency at Re = 155.2 and associated fifth or final slope change marks the origin of the final non-lock-in response branch, DS II. The vibrations in the TB and the initial part of DS II are quasi-periodic such that $St_Y < St_{C_l}$ in TB and $St_Y = St_{C_l}$ in DS II.

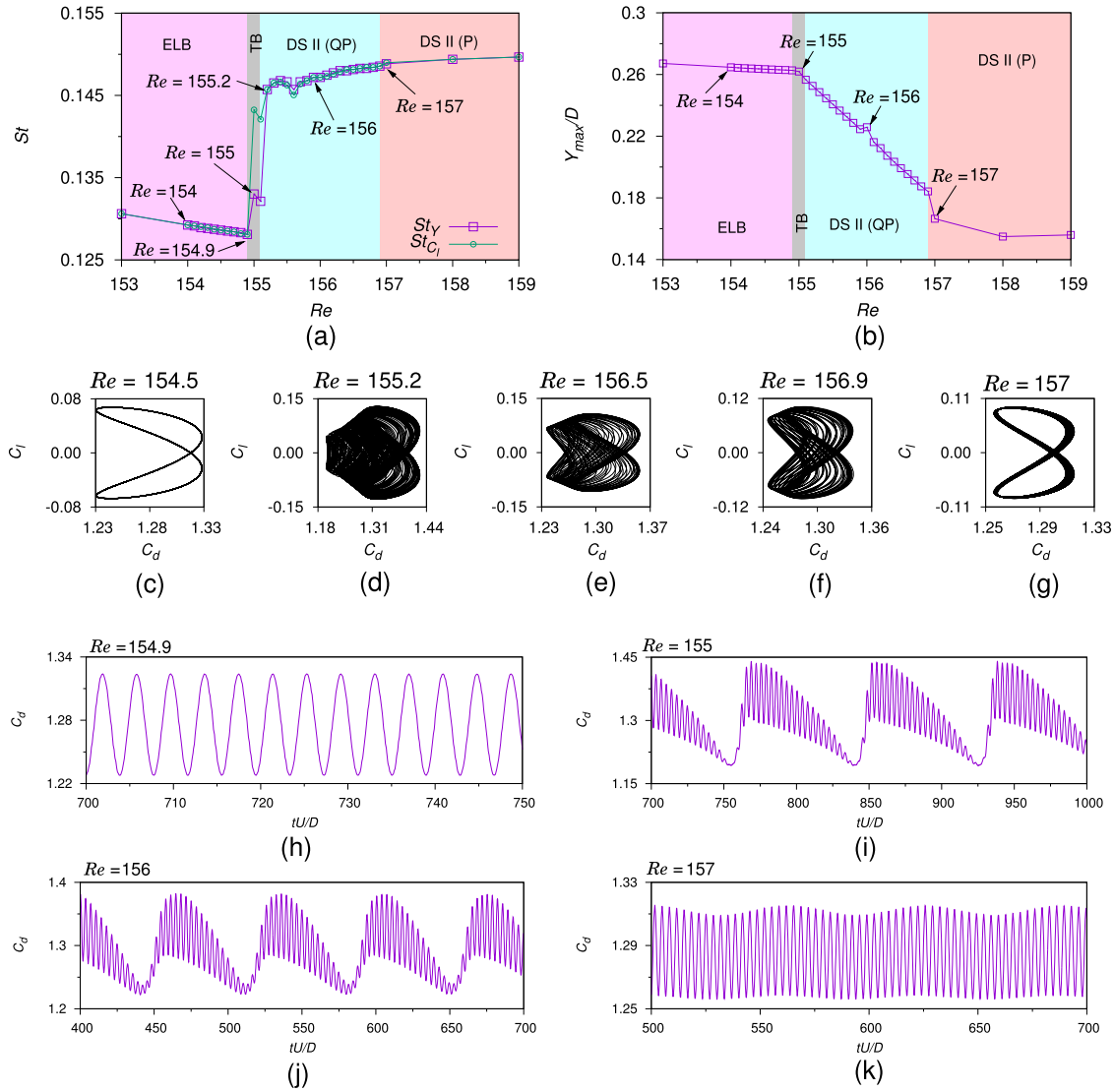

FIG. 6. Undamped *Y*-only VIV of an elliptic cylinder of $AR = \frac{10}{9}$ and m^* = 1: (a) *St*–*Re* and (b) Y_{max}–*Re* relationship close to the end of lock-in. The C_d–C_l Lissajou diagrams at *Re* = (c) 154.5, (d) 155.2, (e) 156.5, (f) 156.9, and (g) 157. Time traces of C_d are shown at *Re* = (h) 154.9, (i) 155, (j) 156, and (k) 157.

Published under license by AIP Publishing

TABLE II. Undamped transverse-only VIV of a thick elliptic cylinder of $AR = \frac{10}{9}$ and $m^* = 1$: summary of the range of response branches. For this case, a total of six transitions are identified.

Range of DS I	Range of IB	Range of LB	Range of ELB	Range of TB	Range of DS II (QP)	Range of DS II (P)
50—52	53–64	65–148	149–154.9	155–155.1	155.2–156.9	157–180

Gross periodicity prevails in the remaining branches including the later part of DS II. The quasi-periodicity at $Re = 155$ and 156 in TB and early DS II, respectively, is reflected via respective C_d–C_l Lissajou diagrams [Figs. 5(c) and 5(e)] as well as power spectra of C_l [Figs. 5(d) and 5(f)].

The decomposition of DS II in its quasi-periodic and periodic segments is analyzed in Fig. 6. The third discontinuous jump in St_Y occurring at $Re = 155.2$ [Fig. 6(a)] signifies the commencement of a response branch in which the slope of St_Y does not exhibit any appreciable variation until $Re = 180$. This is the second regime of desynchronization, the initial segment of which relates to quasi-periodicity and the terminal part to periodicity. In may be noted that discontinuous jump in St_Y at $Re = 155.2$ does not necessarily translate to a discontinuity in Y [Fig. 6(b)]. Thus, identification of the quasi-periodic DS II branch does not appear to be possible from response and also from frequency (constant slope of St_Y over $155.2 \le Re \le 180$). The undamped Y-only VIV of the elliptic cylinder, therefore, represents an instance where the quasi-periodic and periodic segments of DS II construct a continuous curve with $St_Y = St_{C_l}$ throughout. This renders the demarcation of the boundary between DS II (QP) and DS II (P) segments not possible via the method of Kumar *et al.* (2018b). To locate the boundary, the time traces of fluid forces as well as phase portraits are employed. For $155.2 \le Re \le 156.9$, the C_d–C_l Lissajou diagrams [Figs. 6(d)–6(f)] clearly reveal quasi-periodicity while $St_Y = St_{C_l}$. This regime of Re forms the quasi-periodic DS II branch. The segment of DS II stretching from $Re = 157$ to 180 is periodic and corresponds to the DS II (P) branch. We are unaware of any prior decomposition of DS II into periodic and quasi-periodic parts. The figure eight profile of C_d–C_l Lissajou diagram [Fig. 6(g)] ascertains periodicity at $Re = 157$. Figures 6(h)–6(k) illustrate the time traces of drag. At $Re = 154.9$, marking the extreme point of the ELB, the time signal reveals periodicity [Fig. 6(h)] as expected from the periodic C_d–C_l Lissajou diagram at $Re = 154.5$ [Fig. 6(c)] belonging to the same branch. A quasi-periodic C_d signal [Fig. 6(i)] with $St_Y \neq St_{C_l}$ [Fig. 6(a)] and associated jump discontinuity at $Re = 155$ essentially suggests that $Re = 155$ is not located in the same branch as $Re = 154$; it is rather part of a separate branch TB that, unlike ELB, is quasi-periodic. While, at $Re = 156$ [Fig. 6(j)], the drag shows a similar trend as at $Re = 155$, the St–Re segment containing this point relates to a further jump discontinuity, and hence, $Re = 156$ is part of a different branch, i.e., quasi-periodic DS II. Beating is a phenomenon associated with low amplitude vibrations where the fluid-structure system contains multiple frequencies (Willden and Graham, 2006). This generally occurs close to the lock-in boundaries. The C_d signals for $Re = 155$ and 156 contain beats. Finally, periodicity is recovered at $Re = 157$ [Fig. 6(k)] and constancy of slope of the St–Re profile indicates transition from the quasi-periodic to periodic segment of the same branch, i.e., DS II.

Table II summarizes the range of Re for each response branch. It is evident that the extent of ELB is the largest among all three newly identified branches but significantly smaller than those of the fundamental branches, i.e., IB and particularly LB. The cylinder response shown in Fig. 7 for $Re = 50$–180 illustrates all the branches and transitions. The response in the ELB is smaller than the response in the LB and hovers around $0.3D$. The unique feature of response for low m^* is that the transition of moderate amplitude VIV toward the closure of lock-in to periodic decoherence via DS II (QP) is continuous as against a sharp drop of Y generally noted for high m^* (Fig. 4 of Navrose *et al.*, 2014 for $m^* = 10$).

2. The wake modes and mean surface pressure

Williamson and Roshko (1988) conducted extensive experimental investigations on forced transverse vibrations of a circular cylinder in a towing tank. For several values of oscillation amplitude, the interactions among vortices shed in an oscillation cycle were closely studied. The arrangements of shed vortices as a function of amplitude and wavelength/reduced speed were presented in a vortex synchronization map. Certain nomenclature for wake modes of vortex-formation, such as 2S, C(2S), and P + S was introduced based on the vortex arrangements. By "S" a single vortex and by "P" a pair of opposite-signed vortices were denoted by Williamson and Roshko (1988). Accordingly, the basic Kármán mode of vortex-shedding was

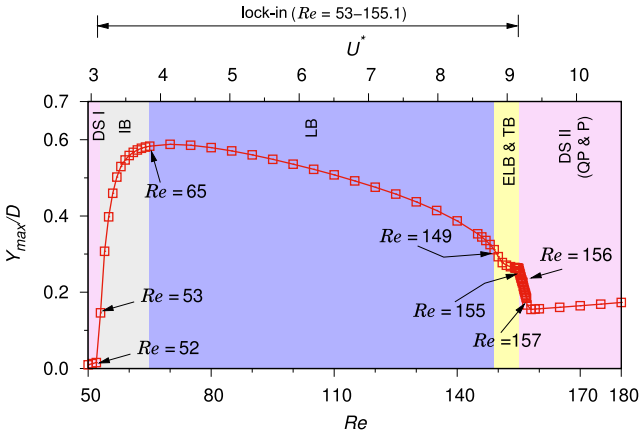

FIG. 7. Undamped transverse-only VIV of a rigid elliptic cylinder of $AR = \frac{10}{9}$ and $m^* = 1$ over $Re = 50$–180: the relationship of response with Re and U^*. The branching of response is illustrated via regimes of varying colors. The newly identified branches ELB and TB were erroneously considered by Sourav and Sen (2017) as part of the lower branch.

Published under license by AIP Publishing

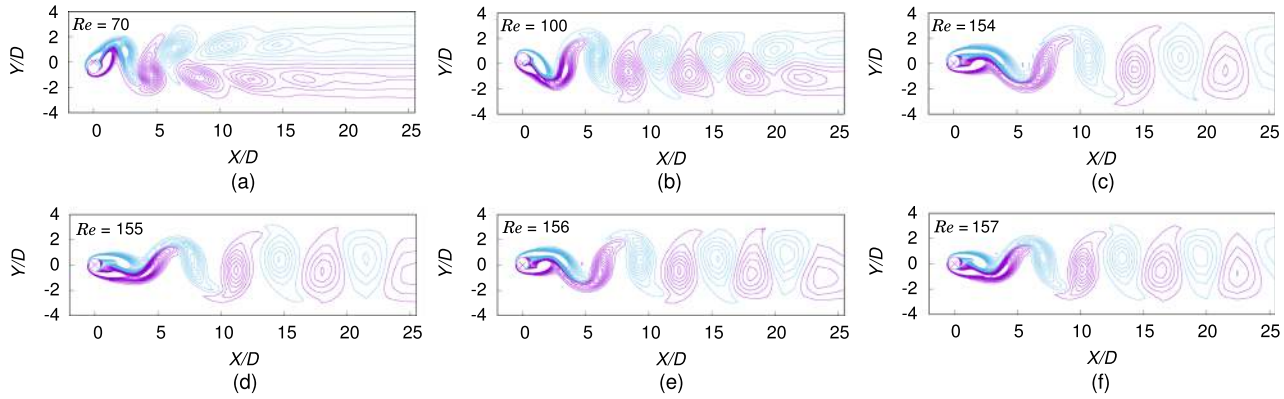

FIG. 8. Undamped *Y*-only VIV of an elliptic cylinder of $AR = \frac{10}{9}$ and $m^* = 1$: the wake modes of vortex-formation at *Re* = (a) 70 in LB, (b) 100 in LB, (c) 154 in ELB, (d) 155 in TB, (e) 156 in DS II (QP), and (f) DS II (P). The wake mode is C(2S) for panels (a) and (b), while for the rest, it is 2S. The origin of the fixed coordinate system is indicated by ×.

designated by 2S. The C(2S) mode forms due to coalescence of like sign vortices of 2S mode. Hence, 2S corresponds to the basic mode in which a pair of vortices of opposite sign are shed in an oscillation cycle. The wake mode is a function of amplitude and reduced speed. For high amplitude transverse oscillations, the wake mode is C(2S) as noted at *Re* = 70 [Fig. 8(a)] and 100 [Fig. 8(b)], both belonging to LB. Toward the closure of lock-in, where the amplitude is low, i.e., the response is of the order of 0.2*D*, the wake mode is 2S irrespective of the response branch. This is supported by Figs. 8(c)–8(f) corresponding to ELB, TB, DS II (QP), and DS II (P), respectively. Thus, the wake modes and response branches appear uncorrelated for the VIV of a thick elliptic cylinder in the low *Re* laminar vortex-shedding regime.

The time-averaged surface pressure, C_p, is illustrated in Fig. 9 for *Re* = 154, 155, 156, and 157 belonging to LB, ELB, TB, and DS II (QP), respectively. While multiple transitions occur over this narrow range of *Re*, the C_p plots overlap and reveal symmetry about the base point. This symmetry is consistent with the anti-symmetric

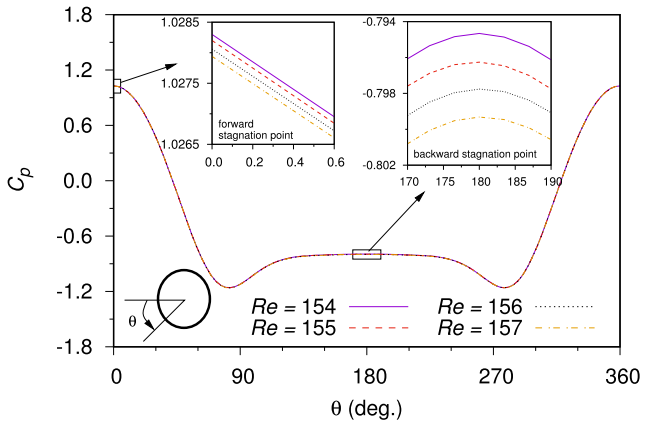

FIG. 9. Undamped *Y*-only motion of an elliptic cylinder of $AR = \frac{10}{9}$ and $m^* = 1$: the distribution of mean surface pressure for *Re* = 154, 155, 156, and 157.

2S wake vortex mode resolved at these *Re*. It may be noted that the time-averaged values of lift and *Y* response for these *Re* are zero [Figs. 16(c)–16(f)].

B. Effect of damping on branching for SDOF motion

The role of damping in altering the response branches for SDOF VIV, if it indeed does so, is tested next. The damped *Y*-only motion is investigated for $\zeta = 0.044$. In context of VIV of a thick elliptic cylinder of $m^* = 1$, Sourav and Sen (2017) demonstrated that damping eliminates quasi-periodicity. The dependence of oscillation frequency on *Re* is depicted via Fig. 10(a) both for undamped and damped *Y*-only VIV. In the early state of lock-in, the damped frequency is lower than its undamped counterpart and the trend alters appreciably toward the end of lock-in. Overall, the damping does not appear to affect the range of lock-in significantly. The "V" region of undamped frequency is largely shortened due to damping, and the appearance of an attenuated "V" toward the upper boundary of LB is quite clear from the figure. An enlarged view of this "V" region is shown in the inset of Fig. 10(a). The LB terminates at *Re* = 152. A slope change at *Re* = 153 indicates the beginning of ELB at this *Re*. For clarity, the frequency curve for $\zeta = 0.044$ is shown in Fig. 10(b). The lowest point of the "V" corresponding to *Re* = 154 marks the end of ELB as well as the upper boundary of lock-in. The next slope change at *Re* = 155 signifies that DS II has begun. DS II is found to be essentially periodic. It is noteworthy that the ELB → DS II transition does not involve a jump but a single change of slope. Thus, the quasi-periodic TB and DS II (QP) do not form. For the VIV with low m^*, damping, therefore, does remove the quasi-periodicity and VIV turns grossly periodic. The terminal point of the ELB is chosen as a representative point at which we show the C_d–C_l phase diagram. The figure eight shape of the diagram ensures the periodic nature of flow and VIV. The response due to damping is smaller in lock-in and higher in non-lock-in regimes as compared to the undamped response [Fig. 10(c)].

A summary of the VIV/flow quantities for undamped as well as damped VIV is provided in Table III. The maximum amplitude due to damping drops approximately by 8%. Compared to undamped

Published under license by AIP Publishing

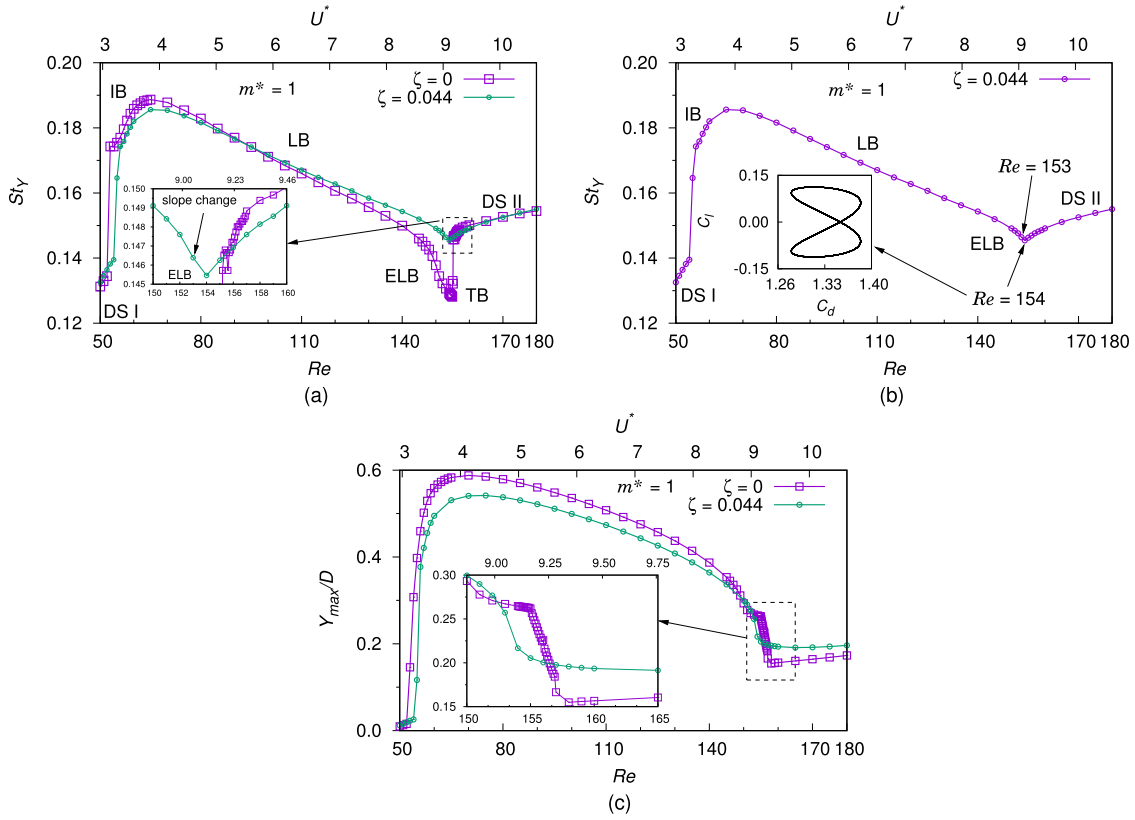

FIG. 10. Transverse-only vortex-induced vibrations of a thick elliptic cylinder of $AR = \frac{10}{9}$ and $m^* = 1$: effect of damping on (a) frequency and (c) response. For clarity, panel (b) separately shows the damped frequency shown in (a). The small "V" shaped region in (a) and (b) indicates that LB transits to DS II through ELB.

VIV, attainment of the peak response also gets delayed. In both cases, the largest value of St is attained at the onset of LB. The lowest value of St denotes the closure of lock-in for damped motion and upper boundary of the resonance branch ELB for undamped motion. The value of St is larger in the former case. With damped VIV, the extent of ELB shrinks noticeably.

C. Effect of oscillator cross section on branching for SDOF motion

The newly identified low amplitude response branches do not appear for the undamped 2-DOF VIV of a circular cylinder ($AR = 1$) of $m^* = 1$ [see Fig. 6.2(a) of Prasanth, 2009]. As discussed in Subsection V D, this behavior is identical to that of the thick elliptic cylinder of $AR = \frac{10}{9}$. To understand the effects of oscillator shape on branching, the response of the circular cylinder for undamped Y-only motion is analyzed. The frequency and response characteristics are shown in Figs. 11(a) and 11(b), respectively, along with the results for the $AR = \frac{10}{9}$ cylinder. Lowering the AR shortens the width of the lock-in regime. It is also found that the third change of slope marking the initiation of ELB for $AR = 1$ occurs at a Reynolds number of 129, a value quite lower compared to $Re = 149$ for $AR = \frac{10}{9}$ [Fig. 11(a)]. Post the ELB, an abrupt jump in frequency marks the commencement of DS II that is periodic in nature. The quasi-periodic branches TB and DS II (QP) do not exist for the circular cylinder.

TABLE III. Transverse vortex-induced vibrations of an elliptic cylinder of $AR = \frac{10}{9}$ and $m^* = 1$: summary of the key characteristic quantities for undamped ($\zeta = 0$) and damped ($\zeta = 0.044$) vibrations.

					Onset of lock-in			Closure of lock-in			
ζ	Y_{max}/D	Re for Y_{max}/D	St_{max}	St_{min}	Re	St	Y_{max}/D	Re	St	Y_{max}/D	Re range of ELB
0	0.5878	70	0.1887	0.1281	53	0.1743	0.1459	155.1	0.1321	0.2566	149–154.9
0.044	0.5417	75	0.1856	0.1463	55	0.1646	0.1167	154	0.1454	0.2166	153–154

Published under license by AIP Publishing

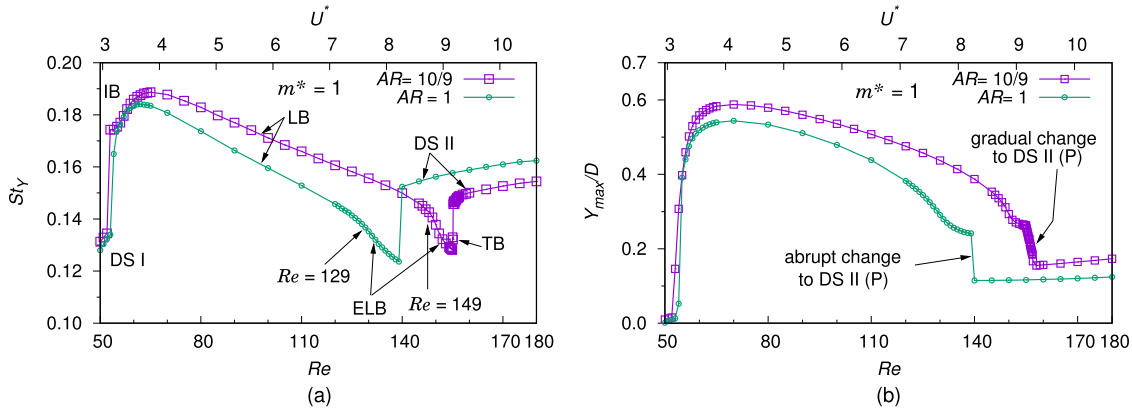

FIG. 11. Effect of cross section on response branching of elliptic cylinders of $m^* = 1$ executing transverse-only VIV: the relationship of (a) frequency and (b) response with Re and U^* for $AR = \frac{10}{9}$ and 1. For $AR = 1$, the LB → DS II transition occurs through the ELB and the quasi-periodic branches TB and DS II (QP) do not appear.

D. Branching for undamped X–Y-motion with $m^* < 10$: Identification of "extended initial branch" or EIB

We first test if lowering the mass ratio below 10 alters the branching of undamped 2-DOF VIV discussed in Subsection I D. To this end, the frequency and response of the $AR = \frac{10}{9}$ cylinder is analyzed for mass ratios of 1 and 5. For $m^* = 5$, Fig. 12(a) depicts the frequency characteristics and shows the Re locations marking transitions. A total of three slope changes or branch transitions at Re = 73, 80, and 138, respectively, are very clear in this figure. The first transition at $Re = 73$ implies the onset of lock-in as well as initiation of IB. The response is made of the four fundamental branches that appear in the following sequence: DS I, IB, LB, and DS II (labeled in the figure). The DS II is periodic. A departure from the frequency patterns of $m^* = 5$ and 10 is seen for $m^* = 1$ in the region next to the onset of lock-in [Fig. 12(b)]. In this case, the transition of IB to LB is continuous as opposed to the discontinuous transition via a jump for higher m^* values of 5 and 10. The first change of slope for $m^* = 1$ is noted at $Re = 53$. Unlike for higher mass ratios, a dip in frequency is noted thereafter, followed by the second slope change at $Re = 56$. This regime of decaying frequency stretching from $Re = 53$ to $Re = 55$ is the initial branch. Subsequent to this, the frequency continues to rise smoothly until it attains its peak value at $Re = 65$. The region bounded by $Re = 57$ and 64 represents a new response branch that substitutes the discontinuous jump found for $m^* = 5$ and 10. Since this branch is an extension of the IB that meets the LB, we define this branch as "extended initial branch" (EIB). The change of slope for the third time at $Re = 65$ signifies the commencement of LB. A final slope change occurs at $Re = 169$ and indicates LB → DS II transition. The last two slope changes at $Re = 65$ and 169 imply that the LB ranges from $Re = 65$ to 168 and DS II from $Re = 169$ to 180. Therefore, for $m^* = 5$ and 10, the response consists of all four of the basic branches, i.e., DS I, IB, LB, and DS II, which are captured for low Re VIV of a circular/thick elliptic cylinder. For $m^* = 1$, one additional branch, i.e., EIB, contributes to the branching. A zoomed-in view of Fig. 12(c) illustrates the details of frequency curve in the vicinity of IB and EIB. The identification of all the response branches for $m^* = 1$ appears difficult, if not impossible, from the X_{rms}–Re variation presented in Fig. 12(d). The existence of EIB as well as the locations of transitions in between the IB and LB cannot be determined from the X_{rms} profile. However, the quasi-periodic segment of the LB is identified as the horn in X_{rms} stretching over $Re = 166$–168. The C_d–C_l [Fig. 12(e-i)] and C_l–Y [Fig. 12(e-ii)] phase diagrams ascertain the quasi-periodic nature of flow and VIV at $Re = 168$ marking the termination of lock-in. An out of phase relationship between C_l and Y is also evident from the C_l–Y phase diagram. The associated power spectra of C_l [Fig. 12(e-iii)] and Y [Fig. 12(e-iv)] reveal quasi-periodicity with almost identical value of the dominant frequency. The response for $m^* = 1$, 5, and 10 is compared in Fig. 12(f). The absence of a horn (indicating a rise) in response of $m^* = 5$ toward the upper extremity of synchronization implies that its lower branch does not contain the quasi-periodic component, while those for $m^* = 1$ and 10 do. Besides widening of the range of synchronization with decreasing m^* (Stappenbelt *et al.*, 2007 and Shen and Sun, 2019), a rise in the magnitude of the maximum transverse response is also noted. In addition, the lock-in sets in earlier, and consequently, the peak value of $Y_{\max}$ is attained at lower Re. The extent of response jump marking the IB → LB transition drops with decreasing m^* and is not realized for $m^* = 1$. The transition from IB to EIB is not discernible from the response.

To understand the formation of EIB solely for $m^* = 1$, the oscillation frequency is analyzed for $m^* = 1$, 5, and 10 (Fig. 13). For a fixed cross-sectional area of the oscillator, a reduction in the value of m^* signifies a decrease in the value of oscillator mass; the oscillator thus turns lighter. When subject to a given fluid loading, the lighter cylinder, as compared to the heavier ones, is expected to be more prone to vortex-excited motion. This explains the early (at lower Re or U^*) settling of lock-in as well as higher Y for $m^* = 1$ [Fig. 12(f)]. By considering the value of the stationary vortex-shedding frequency of a bluff body to roughly equal 0.2 over a wide range of Re, Williamson and Roshko (1988) suggested that the fundamental synchronization occurs at $U^* \approx 5$. With $m^* = 1$, the lock-in commences at $Re = 53$ or $U^* = \frac{53}{16.91} = 3.13 < 5$. The corresponding value of the reduced natural frequency or F_N is $\frac{16.91}{53} = 0.3191$, a value well above 0.2. Thus, the oscillation frequency for $m^* = 1$ can never

Published under license by AIP Publishing

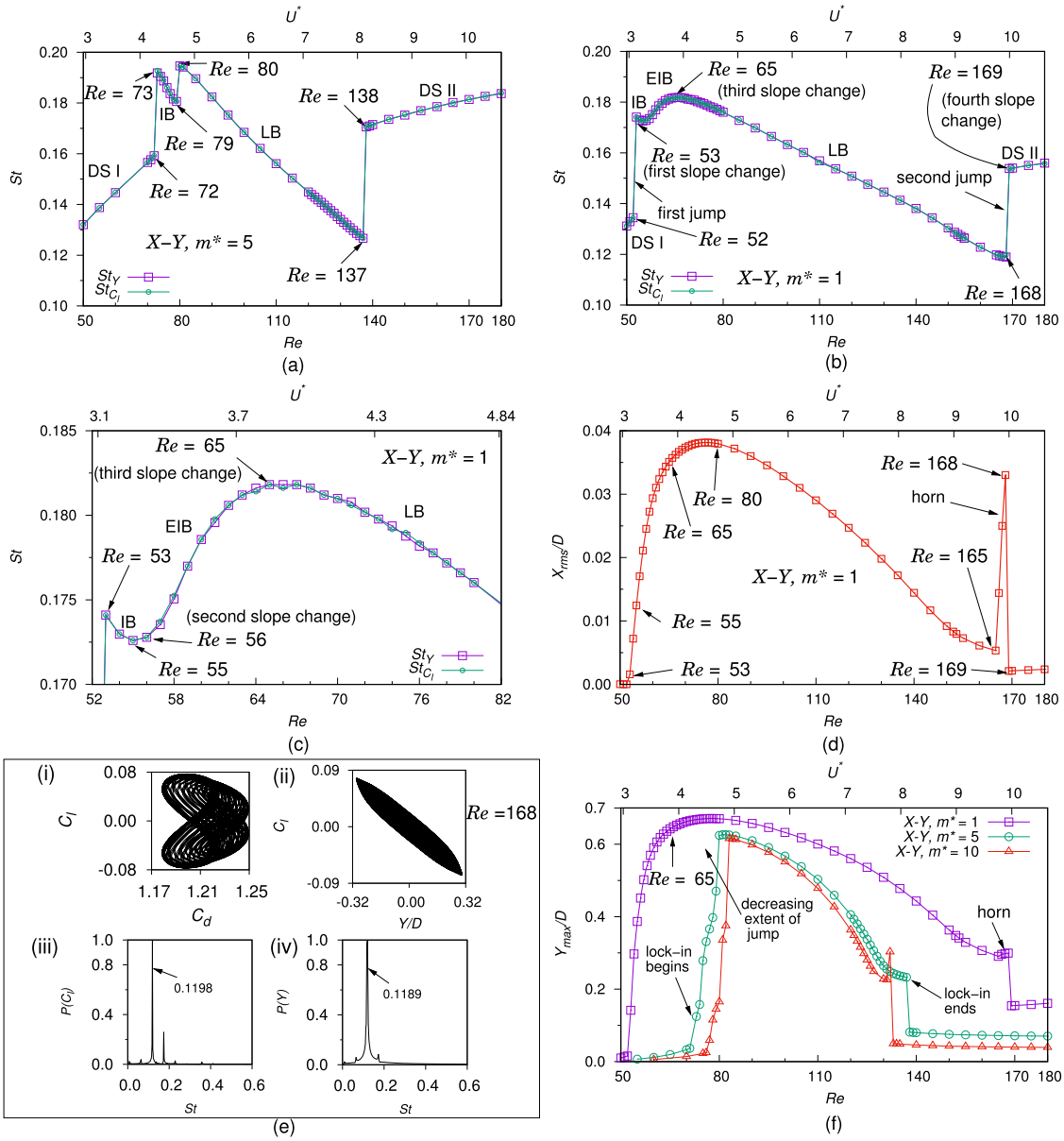

FIG. 12. Undamped 2-DOF VIV of an $AR = \frac{10}{9}$ elliptic cylinder over Re = 50–180: (a) variation of St_Y and St_{C_l} with Re for m^* = 5; (b) variation of St_Y and St_{C_l} with Re for m^* = 1; (c) close-up of (b) showing the details of IB and EIB; (d) the X_{rms}–Re relationship; (e) at Re = 168, (i) C_d–C_l phase diagram, (ii) C_l–Y phase diagram, (iii) power spectrum of C_l, and (iv) power spectrum of Y; and (f) comparison of Y response for m^* = 1, 5, and 10.

reach the F_N value of 0.3191. The value of St_Y at the onset of lock-in, in general, represents the maximum value of St or its close approximation over the entire stretch of lock-in (this is evident from Fig. 13 for m^* = 1, 5, and 10). An early onset of lock-in, thus, renders the St_Y to fall short of corresponding F_N over a significant extent of lock-in. Hence, lock-in for m^* = 1 turns out to be non-classical or soft. Immediately next to the onset of synchronization, St_Y decays with Re, i.e., St_Y, alike F_N, follows an $\frac{1}{Re}$ relationship. Since the lock-in is soft, the value of maximum St_Y for m^* = 1 is low. As Re is increased progressively, the value of U^* approaches 5 corresponding to the fundamental synchronization and the inverse St_Y–Re relationship alters, i.e., the value of St_Y increases. The maximum St_Y signifies the beginning of LB. Two local peaks, therefore, characterize the oscillation frequency of the $AR = \frac{10}{9}$ cylinder: the first one signifying the onset of lock-in and the second one signifying the commencement of LB. Between the onset of lock-in (or first peak of St_Y) and the maximum oscillation frequency close to U^* = 5 (or second peak of St_Y), the oscillation frequency for all m^* initially drops followed

Published under license by AIP Publishing

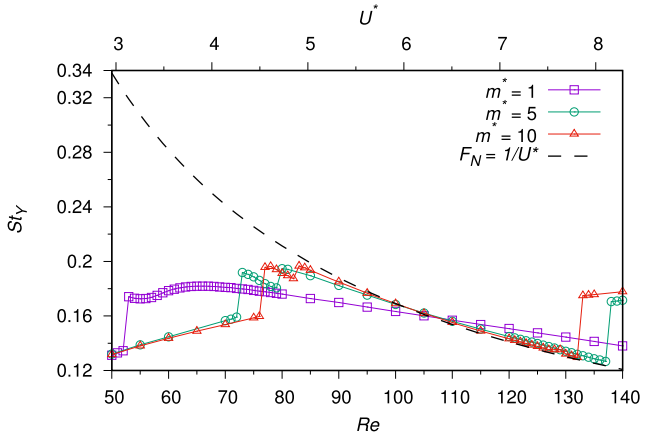

FIG. 13. Undamped transverse-only VIV of an elliptic cylinder of $AR = \frac{10}{9}$: the effect of m^* on the oscillation frequency. The reduced natural frequency $F_N = \frac{16.91}{Re}$ is also plotted.

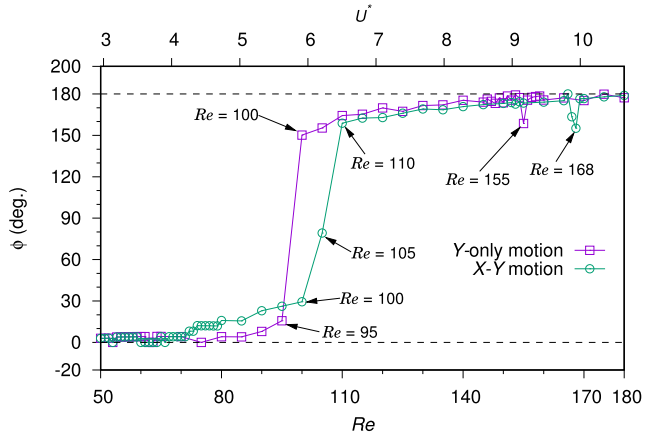

FIG. 15. Undamped VIV of an elliptic cylinder of $AR = \frac{10}{9}$: comparison of the phase between lift and transverse response for SDOF and 2-DOF motions. The transition of response branches are not reflected in the ϕ–Re curves.

by a rise. This signals an intermediate change of slope and possible existence of a branch connecting the IB and LB. For $m^* = 1$, the occurrence of lock-in appears less correlated with F_N, and hence, St_Y need not catch up F_N for lock-in. Because of this, the St_Y–Re curve is relatively flat over a substantial extent of lock-in. This insensitivity of oscillation frequency to F_N for $m^* = 1$ permits the oscillator sufficient range of Re (or U^*) to attain the St_Y value corresponding to the second peak, and hence, the transition from the IB to LB is smooth or continuous. The continuous segment of St_Y corresponds to the EIB. As the m^* (and hence oscillator mass) increases, the VIV is excited at higher Re or U^*. Thus, the range of DS I or the range of Re over which the vortex-shedding (or oscillation) frequency of the vibrating cylinder is close to the vortex-shedding frequency of the stationary cylinder increases. With higher extent of DS I, the lock-in

TABLE IV. Undamped vortex-induced vibrations of an elliptic cylinder of $AR = \frac{10}{9}$ and $m^* = 1$: summary of the key characteristic quantities for Y-only (first row) and X–Y (second row) motions of the cylinder.

					Onset of lock-in			Closure of lock-in		
Motion	Y_{max}/D	Re for Y_{max}/D	St_{max}	St_{min}	Re	St	Y_{max}/D	Re	St	Y_{max}/D
Y-only	0.5878	70	0.1887	0.1281	53	0.1743	0.1459	155.1	0.1321	0.2566
X–Y	0.6703	80	0.1818	0.1188	53	0.1741	0.1415	168	0.1190	0.2995

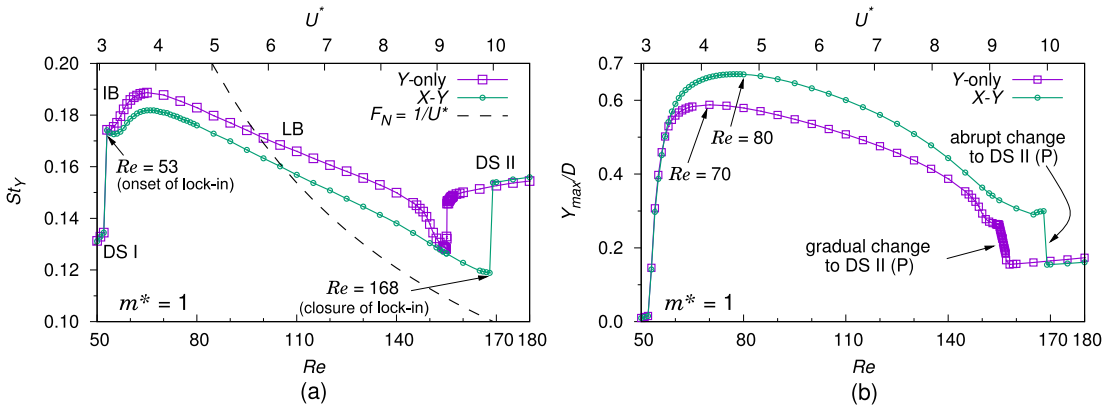

FIG. 14. Undamped VIV of a rigid elliptic cylinder of $AR = \frac{10}{9}$ and $m^* = 1$ over $Re = 50$–180: comparison of (a) oscillation frequency and (b) response for SDOF and 2-DOF motions.

Published under license by AIP Publishing

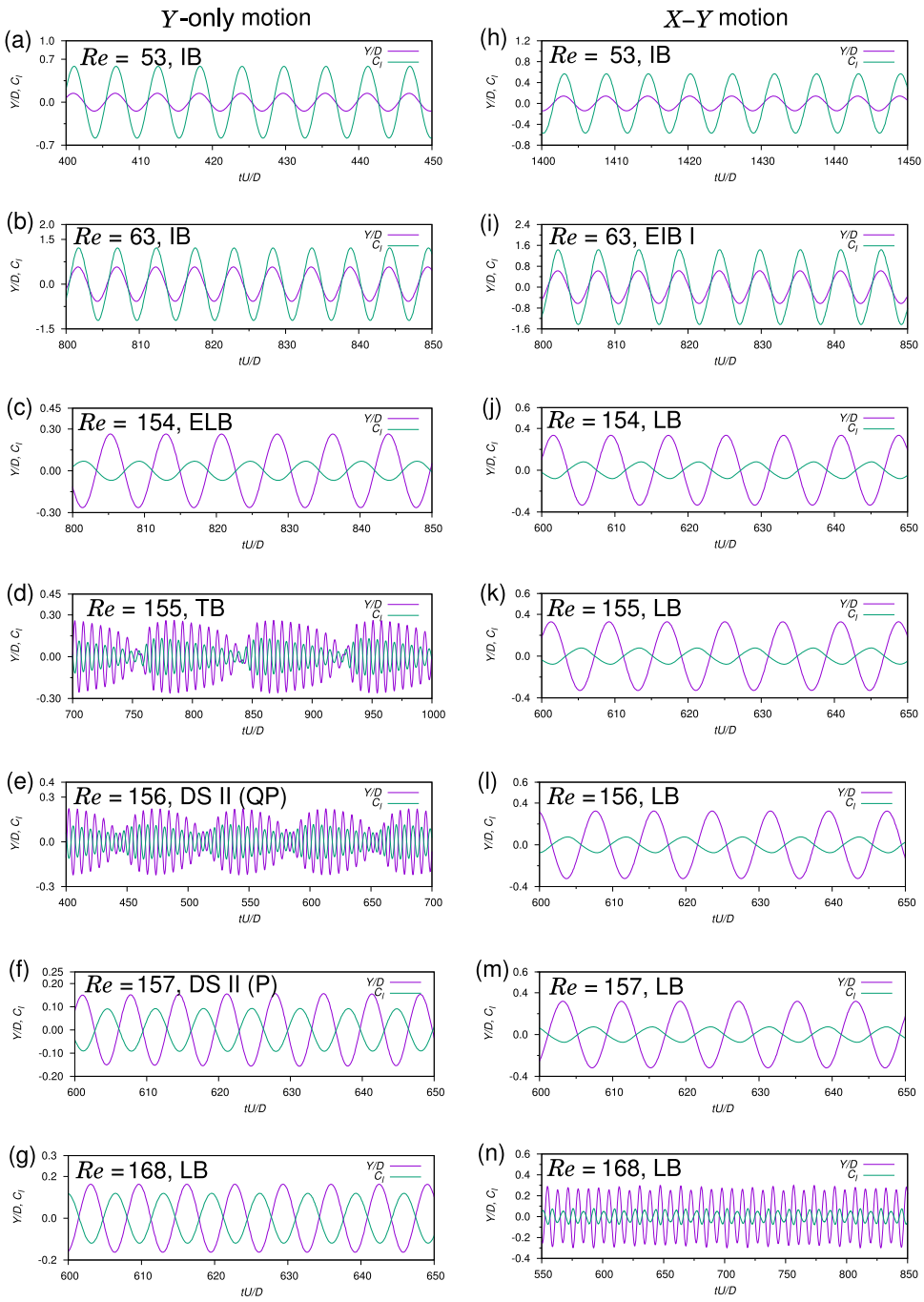

FIG. 16. Undamped Y-only (left column) and X–Y (right column) motion of an elliptic cylinder of $AR = \frac{10}{9}$ and $m^* = 1$: time traces of lift and response at *Re* = [(a) and (h)] 53, [(b) and (i)] 63, [(c) and (j)] 154, [(d) and (k)] 155, [(e) and (l)] 156, [(f) and (m)] 157, and [(g) and (n)] 168.

commences at delayed (higher) reduced speed. Thus, the first peak of St_Y occurs at U^* relatively close to 5 and *Re* or U^* interval between the frequency peaks decays. Next to the initial drop, the St_Y tries to catch up the F_N, and this occurs abruptly owing to gradually shortening interval of *Re* between the St_Y peaks. Thus, a discontinuous jump between the IB and LB precludes the formation of EIB for $m^* = 5$ and 10.

E. Comparison of undamped SDOF and 2-DOF VIV for $m^* = 1$

Concerning undamped 2-DOF VIV of the $AR = \frac{10}{9}$ cylinder in the laminar vortex-shedding regime, Figs. 3 and 12 ensure that the branching behavior is sensitive to m^* for values of mass ratio down to unity. Interestingly, for the same cylinder, the classical two branch

Published under license by AIP Publishing

TABLE V. Summary of response branching for various conditions of structural damping, cylinder aspect ratio, and degree-of-freedom. For each case, the *Re* ranges from 50 to 180. The √ symbol indicates the presence of a branch, while × denotes the absence.

Condition	DS I	IB	EIB	LB	ELB	TB	DS II (QP)	DS II (P)
$Y, AR = \frac{10}{9}, m^* = 1, \zeta = 0$	√	√	×	√	√	√	√	√
$Y, AR = \frac{10}{9}, m^* = 1, \zeta = 0.044$	√	√	×	√	√	×	×	√
$Y, AR = 1, m^* = 1, \zeta = 0$	√	√	×	√	√	×	×	√
X–$Y, AR = \frac{10}{9}, m^* = 1, \zeta = 0$	√	√	√	√	×	×	×	√

(IB and LB) structure prevails for $m^* = 5$ and 10, while an additional branch, i.e., EIB, appears for $m^* = 1$. This justifies our choice of $m^* = 1$ as the reference mass ratio for exploring the effects of individual variables, such as degree-of-freedom, structural damping, and cross section of the oscillator discussed earlier. At high Reynolds numbers, Jauvtis and Williamson (2004) experimentally found that SDOF and 2-DOF free vibrations of a circular cylinder differ appreciably for $m^* \leq 6$. For mass ratios exceeding 6, the differences were less prominent. Following the lead of Jauvtis and Williamson (2004), the characteristics of the VIV with single- and two-degrees-of-freedom are, therefore, expected to be noticeably different for a low mass ratio. The differences are quite obvious from Table IV that lists the salient features for undamped VIV of the $m^* = 1$ cylinder with SDOF and 2-DOF motions. Figure 14(a) compares the frequency and Fig. 14(b) compares the response for these two cases of VIV. Even though lock-in in both cases settles at the same *Re*, inclusion of the in-line degree-of-freedom enhances its range. The magnitude of the peak response increases as well. However, the construction of response with Y-only motion becomes more complex than its X–Y counterpart. In this case, more number of branches (seven against five) are occupied within a shorter stretch of synchronization. The inclusion of in-line motion weakens the soft lock-in behavior, thus extending the upper limit of synchronization of 2-DOF VIV. In this region, St_Y drops with *Re* (or U^*) similar to the way F_N decays with *Re*. The St_Y resides close (with respect to Y-only VIV) to the natural frequency [Fig. 14(a)], and the LB transits directly to DS II. It may be noted that the oscillation/vortex-shedding frequency at the onset of lock-in exceeds its value in DS I and at the closure of lock-in, it falls below its value in DS II. To catch up with F_N, the value of the oscillation frequency for Y-only motion drops toward the closure of lock-in. Since the frequency in the DS regimes is practically identical for a given m^*, a subsequent rise in St_Y is essential. The terminal fall and rise of St_Y for SDOF VIV involve multiple changes of slope and form additional response branches.

The phase angle, ϕ, between lift and transverse response for Y and X–Y motion is compared in Fig. 15. In either case, the branch transitions are not reflected in the ϕ–*Re* variation. For $m^* = 1$ cylinder, the undamped Y-only VIV is quasi-periodic over a short range of *Re*. This range (*Re* = 155–156.9) brackets the TB as well as DS II (QP). The motion is periodic for the rest of *Re*. The DS II (QP) segment of quasi-periodicity belongs to the non-locked-in regime. For undamped 2-DOF VIV with the same m^*, quasi-periodicity appears at relatively higher *Re*, i.e., it exists over a narrow interval of *Re* stretching from *Re* = 166 to 168 where *Re* = 168 marks the closure of lock-in. As revealed in Fig. 16, the time traces for periodic VIV are very similar, irrespective of the degree-of-freedom. This implies that the identification of the IB → EIB transition is not possible from the time traces of forces and response. This fact can be appreciated by considering Figs. 16(h) and 16(i) for *Re* = 53 and 63, respectively. Figure 16 is constructed by combining the time histories of C_l and Y for both DOFs at representative Reynolds numbers characteristic to various response branches. For Y-only VIV, the quasi-periodic C_l and Y signals exhibit beating [Fig. 16(d) at *Re* = 155 and Fig. 16(e) at *Re* = 156]. The power spectra of lift signals for *Re* = 155 [Fig. 5(d)] and *Re* = 156 [Fig. 5(e)] both contain significant spectral content. For 2-DOF motion at *Re* = 168, the time traces reveal quasi-periodicity [Fig. 16(n)], but the spectral content in C_l is relatively low [Fig. 12(e-iii)]. The signals are weakly quasi-periodic and beating disappears.

F. Summary of branching

The response branches pertaining to various conditions are summarized in Table V. This summary clearly indicates that the EIB does not appear with single-degree-of-freedom VIV, while the ELB, TB, and DS II (QP) are characteristic to low m^* transverse motion alone.

VI. CONCLUSIONS

Irrespective of the degree-of-freedom, the response branching of a circular cylinder of $m^* \approx 10$ at low *Re* is invariably constituted of two classical branches, the initial and lower. The degree-of-freedom assumes importance in modifying the branching when the mass ratio is reduced to unity. This aspect of VIV highlighting the close connections among response branching, mass ratio, and degree-of-freedom is unavailable in the literature. In this study, stabilized space-time finite-element computations are performed in two-dimensions and the branching behavior of response analyzed over *Re* = 50–180. A thick elliptic cylinder of aspect ratio $\frac{10}{9}$, which is geometrically very similar to a circular cylinder, is considered as the oscillator. With undamped two-degrees-of-freedom motion for $m^* = 1$, a new response branch linking the initial and lower branches is identified. This branch is named as the extended initial branch. The EIB forms out of non-classical resonance characteristic to a low mass ratio for which $St_Y \ll F_N$. The branching turns even more diversified when the $m^* = 1$ cylinder is constrained to have undamped transverse-only motion. Under this condition, the classical two-branch (initial and lower) response at low *Re* undergoes fundamental alterations. An unforeseen frequency variation close to the upper extremity of synchronization is observed.

Published under license by AIP Publishing

Two successive slope changes and a discontinuous jump in oscillation frequency underlines the existence of three additional constituent branches. These low amplitude branches have been designated as the extended lower branch, terminal branch, and quasi-periodic second regime of desynchronization. The wake mode in each of these branches is 2S. These branches disappear in the presence of in-line degree-of-freedom. The VIV is essentially periodic, barring the TB and DS II (QP), where quasi-periodicity dominates the flow and body motion. Structural damping shortens the periodic ELB and removes the quasi-periodic TB and DS II (QP). For undamped Y-only motion of a circular cylinder, the ELB is found to exist, while its TB and DS II (QP) counterparts do not form.

REFERENCES

Amandolese, X. and Hemon, P., "Vortex-induced vibration of a square cylinder in a wind tunnel," C. R. Mec. **338**, 12–17 (2010).

Anagnostopoulos, P. and Bearman, P. W., "Response characteristics of a vortex excited cylinder at low Reynolds number," J. Fluids Struct. **6**, 39–50 (1992).

Bahmani, M. H. and Akbari, M. H., "Effects of mass and damping ratios on VIV of a circular cylinder," Ocean Eng. **37**, 511–519 (2010).

Bearman, P. W., "Vortex shedding from oscillating bluff bodies," Annu. Rev. Fluid Mech. **16**, 195–222 (1984).

Blackburn, H. M., Govardhan, R. N., and Williamson, C. H. K., "A complementary numerical and physical investigation of vortex-induced vibration," J. Fluids Struct. **15**(3-4), 481–488 (2000).

Blevins, R. D., *Flow-Induced Vibration* (Van Nostrand Reinhold, New York, 1990).

Brika, D. and Laneville, A., "Vortex-induced vibrations of a long flexible circular cylinder," J. Fluid Mech. **250**, 481–508 (1993).

Carberry, J., Govardhan, R., Sheridan, J., Rockwell, D., and Williamson, C. H. K., "Wake states and response branches of forced and freely oscillating cylinders," Eur. J. Mech.: B/Fluids **23**, 89–97 (2004).

Feng, C. C., "The measurement of cortex induced effects in flow past stationary and oscillating circular and D-section cylinders," M.Sc. thesis, The University of British Columbia, Vancouver, BC, Canada, 1968.

Govardhan, R. and Williamson, C. H. K., "Modes of vortex formation and frequency response of a freely vibrating cylinder," J. Fluid Mech. **420**, 85–130 (2000).

Jauvtis, N. and Williamson, C. H. K., "Vortex-induced vibration of a cylinder with two degrees of freedom," J. Fluids Struct. **17**, 1035–1042 (2003).

Jauvtis, N. and Williamson, C. H. K., "The effect of two degrees of freedom on vortex-induced vibration at low mass and damping," J. Fluid Mech. **509**, 23–62 (2004).

Jiao, H. and Wu, X., "Free vibration predicted using forced oscillation in the lock-in region," Phys. Fluids **30**, 113601-1–113601-12 (2018).

Khalak, A. and Williamson, C. H. K., "Dynamics of a hydroelastic cylinder with very low mass and damping," J. Fluids Struct. **10**, 455–472 (1996).

Khalak, A. and Williamson, C. H. K., "Fluid forces and dynamics of a hydroelastic structure with very low mass and damping," J. Fluids Struct. **11**, 973–982 (1997).

Khalak, A. and Williamson, C. H. K., "Motions, forces and mode transitions in vortex-induced vibrations at low mass-damping," J. Fluids Struct. **13**, 813–851 (1999).

Klamo, J. T., Leonard, A., and Roshko, A., "The effects of damping on the amplitude and frequency response of a freely vibrating cylinder in cross-flow," J. Fluids Struct. **22**, 845–856 (2006).

Kou, J., Zhang, W., Liu, Y., and Li, X., "The lowest Reynolds number of vortex-induced vibrations," Phys. Fluids **29**, 041701-1–041701-7 (2017).

Kumar, D., Mittal, M., and Sen, S., "Modification of response and suppression of vortex-shedding in vortex-induced vibrations of an elliptic cylinder," Int. J. Heat Fluid Flow **71**, 406–419 (2018a).

Kumar, D., Singh, A. K., and Sen, S., "Identification of response branches for oscillators with curved and straight contours executing VIV," Ocean Eng. **164**, 616–627 (2018b).

Kumar, S., Navrose, and Mittal, S., "Lock-in in forced vibration of a circular cylinder," Phys. Fluids **28**, 113605-1–113605-15 (2016).

Leontini, J. S., Griffith, M. D., Jacono, D. L., and Sheridan, J., "The flow-induced vibration of an elliptical cross-section at varying angles of attack," J. Fluids Struct. **78**, 356–373 (2018).

Leontini, J. S., Thompson, M. C., and Hourigan, K., "The beginning of branching behaviour of vortex-induced vibration during two-dimensional flow," J. Fluids Struct. **22**, 857–864 (2006).

Li, X., Lyu, Z., Kou, J., and Zhang, W., "Mode competition in galloping of a square cylinder at low Reynolds number," J. Fluid Mech. **867**, 516–555 (2019).

Mittal, S. and Kumar, V., "Finite element study of vortex-induced cross-flow and in-line oscillations of a circular cylinder at low Reynolds numbers," Int. J. Numer. Methods Fluids **31**, 1087–1120 (1999).

Mittal, S. and Kumar, V., "Flow-induced oscillations of two cylinders in tandem and staggered arrangements," J. Fluids Struct. **15**, 717–736 (2001).

Mittal, S. and Tezduyar, T. E., "Massively parallel finite element computation incompressible flows involving fluid-body interactions," Comput. Methods Appl. Mech. Eng. **112**, 253–282 (1994).

Navrose, Yogeswaran, V., Sen, S., and Mittal, S., "Free vibrations of an elliptic cylinder at low Reynolds numbers," J. Fluids Struct. **51**, 55–67 (2014).

Nemes, A., Zhao, J., Jacono, D. L., and Sheridan, J., "The interaction between flow-induced vibration mechanisms of a square cylinder with varying angles of attack," J. Fluid Mech. **710**, 102–130 (2012).

Prasanth, T. K., "Vortex-induced vibration at low Reynolds numbers," Ph.D. thesis, Indian Institute of Technology Kanpur, India, 2009.

Prasanth, T. K. and Mittal, S., "Vortex-induced vibrations of a circular cylinder at low Reynolds numbers," J. Fluid Mech. **594**, 463–491 (2008).

Saad, Y. and Schultz, M. H., "GMRES: A generalized minimal residual algorithm for solving non-symmetric linear systems," SIAM J. Sci. Stat. Comput. **7**, 856–869 (1986).

Sarpkaya, T., "Hydrodynamic damping, flow-induced oscillations, and biharmonic response," ASME J. Offshore Mech. Arctic Eng. **117**, 232–238 (1995).

Sen, S. and Mittal, S., "Free vibration of a square cylinder at low Reynolds numbers," J. Fluids Struct. **27**, 875–884 (2011).

Sen, S. and Mittal, S., "Effect of mass ratio on free vibrations of a square cylinder at low Reynolds numbers," J. Fluids Struct. **54**, 661–678 (2015).

Sen, S. and Mittal, S., "Free vibrations of a square cylinder of varying mass ratios," Procedia Eng. **144**, 34–42 (2016).

Shen, L. and Sun, Z., "Jump phenomena in vortex-induced vibrations of a circular cylinder at a low Reynolds number," Phys. Fluids **31**, 123605-1–123605-11 (2019).

Singh, S. P. and Mittal, S., "Vortex-induced oscillations at low Reynolds numbers: Hysteresis and vortex-shedding modes," J. Fluids Struct. **20**, 1085–1104 (2005).

Sourav, K., Kumar, D., and Sen, S., "Undamped transverse-only VIV of a diamond cylinder at low Reynolds numbers," Ocean Eng. **197**, 106867-1–106867-22 (2020).

Sourav, K. and Sen, S., "On the response of a freely vibrating thick elliptic cylinder of low mass ratio," J. Appl. Fluid Mech. **10**(3), 899–913 (2017).

Sourav, K. and Sen, S., "Transition of VIV-only motion of a square cylinder to combined VIV and galloping at low Reynolds numbers," Ocean Eng. **187**, 106208 (2019).

Stappenbelt, B., Lalji, F., and Tan, G., "Low mass ratio vortex-induced motion," in Proceedings of the 16th Australasian Fluid Mechanics Conference, Crown Plaza, Gold Coast, Australia, 2007.

Sun, H., Kim, E. S., Nowakowski, G., Mauer, E., and Bernitsas, M. M., "Effect of mass-ratio, damping, and stiffness on optimal hydrokinetic energy conversion of a single, rough cylinder in flow induced motions," Renewable Energy **99**, 936–959 (2016).

Published under license by AIP Publishing

Tezduyar, T. E., Behr, M., and Liou, J., "A new strategy for finite element computations involving moving boundaries and interfaces—The DSD/ST procedure: I. The concept and the preliminary numerical tests," Comput. Methods Appl. Mech. Eng. **94**, 339–351 (1992a).

Tezduyar, T. E., Behr, M., and Mittal, S., "A new strategy for finite element computations involving moving boundaries and interfaces—The DSD/ST procedure: II. Computation of free-surface flows, two-liquid flows, and flows with drifting cylinders," Comput. Methods Appl. Mech. Eng. **94**, 353–371 (1992b).

Willden, R. H. J. and Graham, J. M. R., "Three distinct response regimes for the transverse vortex-induced vibrations of circular cylinders at low Reynolds numbers," J. Fluids Struct. **22**, 885–895 (2006).

Williamson, C. H. K. and Jauvtis, N., "A high-amplitude 2T mode of vortex-induced vibration for a light body in X–Y motion," Eur. J. Mech.: B/Fluids **23**(1), 107–114 (2004).

Williamson, C. H. K. and Roshko, A., "Vortex formation in the wake of an oscillating cylinder," J. Fluids Struct. **2**, 355–381 (1988).

Zhao, J., Leontini, J. S., Jacono, D. L., and Sheridan, J., "Fluid-structure interaction of a square cylinder at different angles of attack," J. Fluid Mech. **747**, 688–721 (2014).

Zhu, H., Zhang, C., and Liu, W., "Wake-induced vibration of a circular cylinder at a low Reynolds number of 100," Phys. Fluids **31**, 073606-1–073606-19 (2019).

Published under license by AIP Publishing